Development of Electroactive Nonaohybrid Cerasomes

（電気活性をもつナノハイブリッドセラソームの開発）

Qiao Yun

March 2014

Doctoral Thesis at Graduate School of Materials Science

Nara Institute of Science and Technology (NAIST), Japan

Contents

Chapter 1. General introduction

1. 1 Organic-inorganic hybrid materials

The concept of organic-inorganic hybrid material has been proposed and became to be a rapid growing research area in materials sciences along with the emergence of conventional soft inorganic chemistry [1-5]. It has attracted much research interest of chemists, physicists, biologists, and materials scientists in fundamental researches and the wide variety of application fields, such as optoelectronics [6-9], biotechnology [10, 11], and so on. Organic-inorganic hybrid nanomaterials play a significant role in the design and growth of commercially available advanced materials. Nowadays, some hybrid products have already entered into the market, for example, TV sets produced by Toshiba，the screen of which was coated with hybrid materials made of silica-zirconia matrix embedded with indigo dyes by sol-gel method [2]; commercial isomers sunscreen SPF 20 with UV pearls contains active organic components encapsulated into more or less porous silica micro-capsules [12]; glassware sold by Spiegelau coated by organically doped sol-gel [13]; and enzymes sold by Fluka entrapped in sol-gel matrix [14].

The fast expansion of research on organic-inorganic hybrids to a large extent resulted from their novel functions superior to individual organic and inorganic materials [1]. However, these innovative properties relied on not only the sum of individual contribution from organic and inorganic constituents but also a large synergistic effect of the two phases through size domain effects and nature of the interfaces [15]. The role of their inner interfaces could be predominant, whose nature

has been used to grossly categorize these materials into two main classes. In class I, organic and inorganic components are embedded through only weak interactions, such as hydrogen bonds, van der Waals or ionic bonds, giving cohesion to the whole structure without covalent bond. On the contrary, in class II materials, the two phases are partly linked together through strong chemical interaction or covalent bond [3, 16].

At the present time, various types of strategies are available for the construction of organic-inorganic hybrid materials [4]. One of the most promising techniques is sol-gel method, which is initially employed to prepare glassy and ceramic inorganic materials. In the last few decades, the great interests were attracted and intense activities were carried out in this method, the major driving forces behind which are one of the unique properties of the sol-gel process, room-temperature procedure. Under such relatively mild conditions, both biomolecules and organic molecules can withstand. [17-19]. However, one seems to difficultly understand the preparation of organic-inorganic hybrid material by sol-gel method without the basic knowledge of sol-gel reactions. In general, the sol-gel process can be divided into two steps, hydrolysis of metal or semimetal alkoxides precursors and condensation reaction of hydroxyl groups and residual alkoxyl groups to produce corresponding metal oxide inorganic material with a three-dimensional framework structure. The popular inorganic components can be used as precursor such as silica, alumina, titania, zirconia and so on. Among these components, silica is the typical one because of the inherent properties of hybrid materials based on the silica matrix. In the case of silicone alkoxide, the whole procedure of sol-gel reaction is described in **Scheme 1-1**. Under ordinary conditions, the hydrolysis proceeds simultaneously with followed condensation reaction. During these processes, some byproducts with low molecular weight are generated for instance,

water and alcohol. Finally, cross-linked silica gel matrix with three-dimensional network is obtained through the repetitive Si-O- bonds. Additionally, both hydrolysis and condensation reaction are dependent on the type of solvent, catalyst, concentration of starting components and temperature [17].

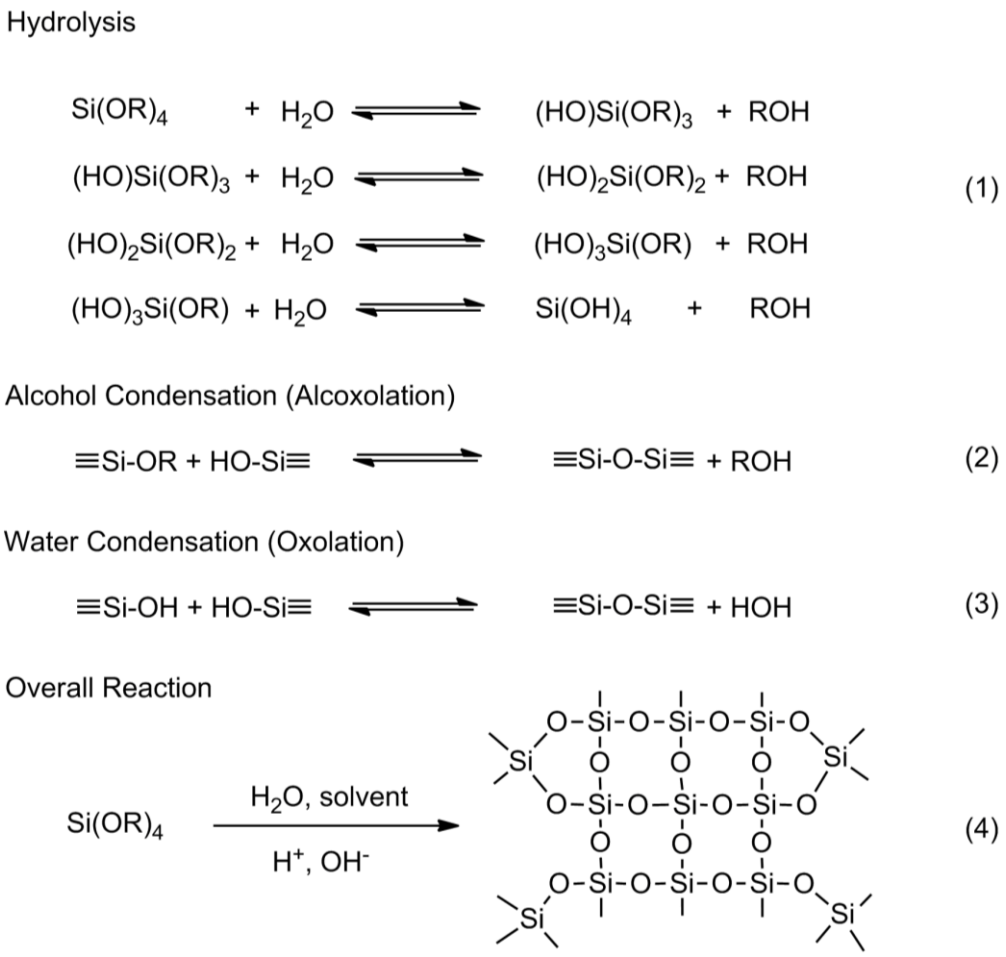

Scheme 1-1. The process of sol-gel reaction [17].

By now, numerous silicon-based organic-inorganic hybrid materials have been developed. The most well-known representatives are the extensive family of mesoporous sieves (M41S) discovered by the researchers at Mobil R&D Corp through surfactant assisted synthesis. One member of the M41S family is named MCM-41[20],

which has a hexagonal arrangement of unidimensional pores varying in size from 1.5 nm to 10 nm depending on organic templates used, addition of auxiliary organic compound and reaction temperature [20]. The synthetic procedure of MCM-41 from tetramethylammonium salt is represented in **Figure 1-1.** The long-chain cationic alkylmethylammonium serves as the organic templates at the beginning and removed by calcinations finally. This innovative approach using supramolecular aggregates of amphiphilic surfactant as structure-directing agent brings about revolution in the area of mesoporous materials. Besides MCM-41, several other members in this family have also been identified, such as MCM-48 exhibiting cubic structure which can be indexed to an Ia3d unit cell [21] and MCM-50 having laminar structure [22].

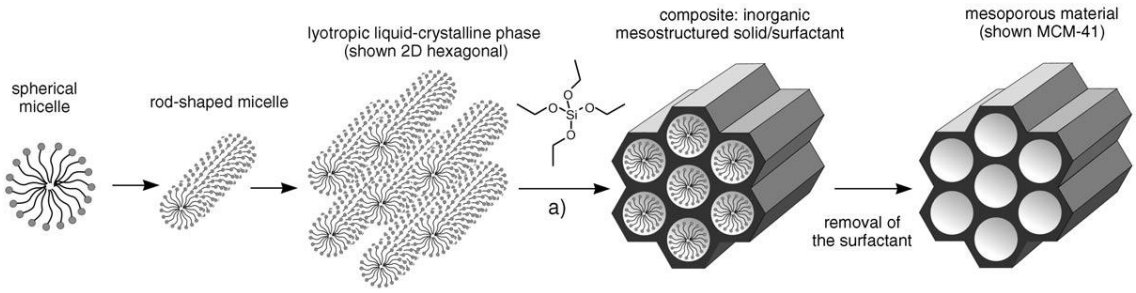

Figure 1-1. Formation of mesoporous materials by structural-directing agents [23].

The surfactant assisted synthesis attracted an extraordinary amount of interest in the scientific community that still continues today since it was created. Nevertheless, the very fact is that most of these composite materials are mainly composed of inorganic components and that the organic components are just used as the template and removed finally. On the contrary, recently, a novel class of layered organic-inorganic nanohybrid materials has been developed, which were composed of amphiphilic molecules in presence of a stable covalent bond between the silicate and the surfactants [24-27]. The procedure of synthesis is exemplified in **Figure 1-2**. On the synthesis of these materials,

the essential self-assemble behaviors perform, which is worth investigating from both scientific and practical viewpoints. It can make the hybrid precursors, organoalkoxysilanes containing a silanol group, covalently attached a hydrophobic tail, to form specific materials with three-dimensional network.

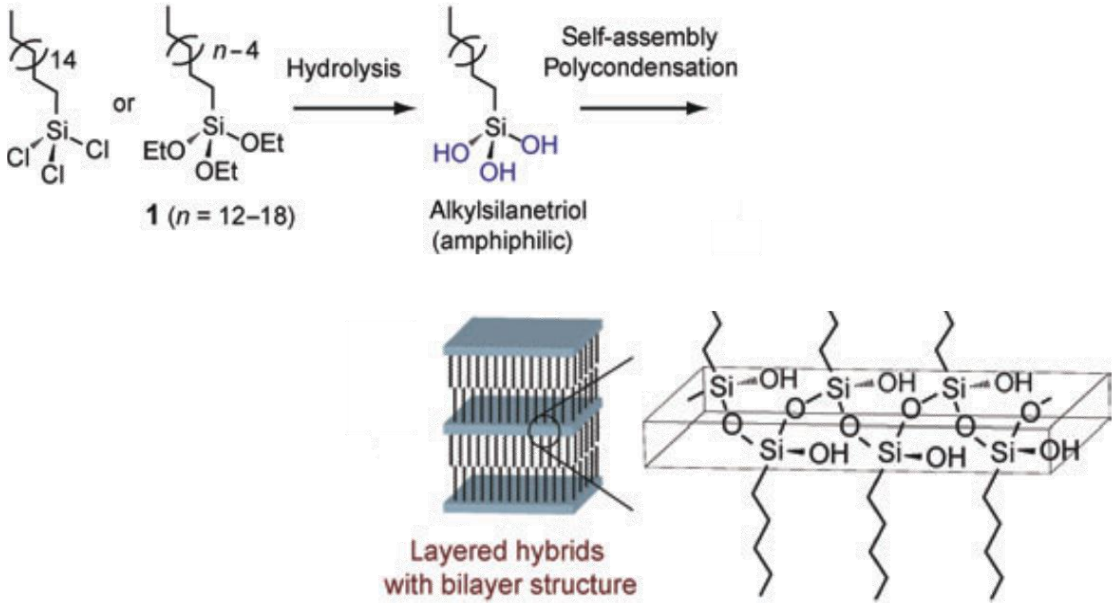

Figure 1-2. Self-assembly of hydrolyzed alkylsilanes into multilayered siloxane-based hybrids [28].

1. 2 Electrochemical application of organic-inorganic hybrids

Bridging chemistry of hybrid organic-inorganic materials with other disciplines are attracted growing interest, and brought out very fruitful and prolific achievement. In particular, the research projects coupling organic-inorganic hybrid nanomaterials based on silicate with the electrochemical properties have been attracted extensive attention in the past two decades [29]. Such silica-based hybrid materials include silica components coated with organic moieties or biomolecules through absorption and followed sol-gel process. Silicates capsulated organic and/or bioorganic species by physical interaction are class I. Whereas interpenetrating ceramic-organic copolymers and organic-inorganic nanocomplex prepared by co-condensation of alkoxysilanes, which are in class II [30].

Because of specific chemical and physiochemical properties, these materials have been used in wide range of application, such as biological and chemical sensors, electropolymerization, spectroelectrochemistry, batteries, and fuel cells. Moreover, the relevant reports about the electrochemical application of organic-inorganic hybrid materials are abundant [31-33].

1. 3 Organic-inorganic nanohybrid cerasomes

Recently, our group developed novel a organic-inorganic hybrid with vesicular structure named cerasome, which is formed through spontaneous self-assembly of organoalkoxysilane lipids along with sol-gel reaction [34]. The cerasome contains an inner aqueous compartment, spherical lipid bilayer membrane like liposome and ceramic-like framework on the surface, denoted in the illustration of **Figure1-3.** Since the only difference between the cerasome and liposome is the additional presence of siloxane network in the former, the cerasome is conceived the combination of liposome and ceramic. As liposome, the size of cerasome is also tunable. By now, cerasomes with various sizes have been designed and prepared by applying conventional methodologies used for preparation of monodispersed liposomes. Generally, two types of preparation methods are employed depending on the water solubility of cerasome forming lipid. One is the direct dispersion method through dispersing cerasome forming lipid with well water solubility into aqueous media [35]. Another one is ethanol sol injection method, which is used for cerasome forming lipids with poor water-solubility. The latter method contains two individual steps [36]. Firstly, the sol of cerasome forming lipids is obtained by incubating lipid in an acidic ethanol solution. Afterward the resulting sol is injected into water under stirring.

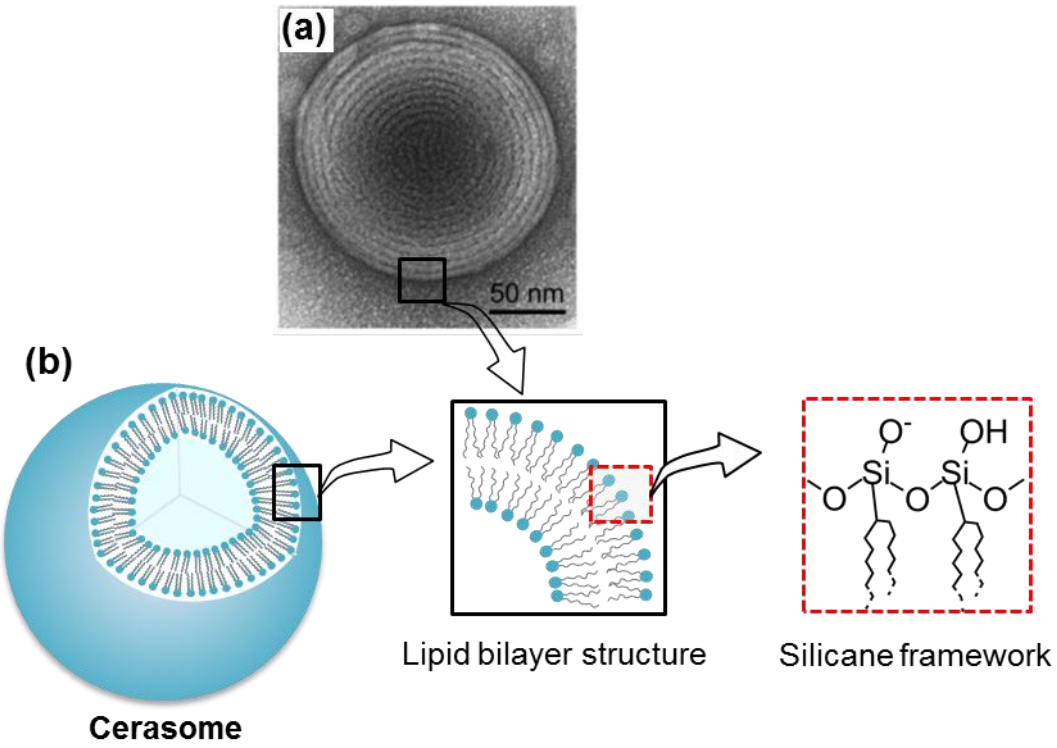

Figure 1-3. Negatively stained TEM image of multiwalled cerasome (a) and schematic drawing of cerasome (b) [37].

Several types of cerasomes have been developed using different kinds of cerasome-forming lipids. The common molecular structure of cerasome forming lipids is shown in **Figure 1-4**. It contains three parts: a connector unit such as a urea or an amide acid residue, an inorganic precursor head moiety and a hydrophobic double-chain segment.

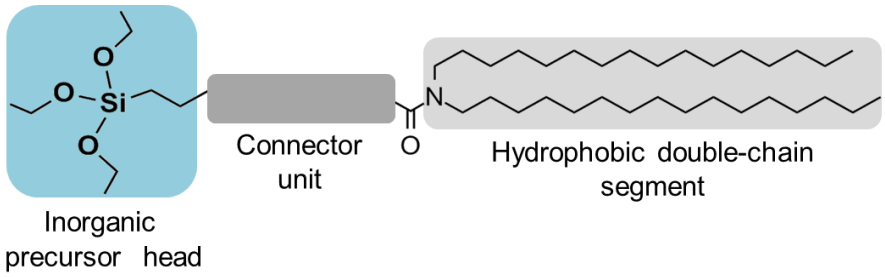

Figure 1-4. Chemical structure of cerasome forming lipid [37].

Owing to the inorganic framework on its surface, the cerasome exhibits a remarkably higher morphological stability as compared with the conventional liposomes. The morphology of cerasomes can be visualized by scanning electron microscopy (SEM) and atomic force microscopy (AFM), however, these microscopic techniques are challenging to observe the liposomes formed by phospholipids with poor stability. **Figure 1-5 (A)** shows SEM image of cerasome prepared by ethanol sol injection method. Our group successfully constructed three-dimensionally packed cerasome assembly on a solid substrate through layer-by-layer assembly method. The AFM images of alternately layer-by-layer assembly films of the anionic and cationic cerasomes are shown in the **Figure 1-5 (B)** [38]. In the contrast, the conventional liposomes are used for preparation of multi-liposomal assembly because the liposomes generally change their vesicular structures when they interact with polyelectrolyte with the opposite charge [39].

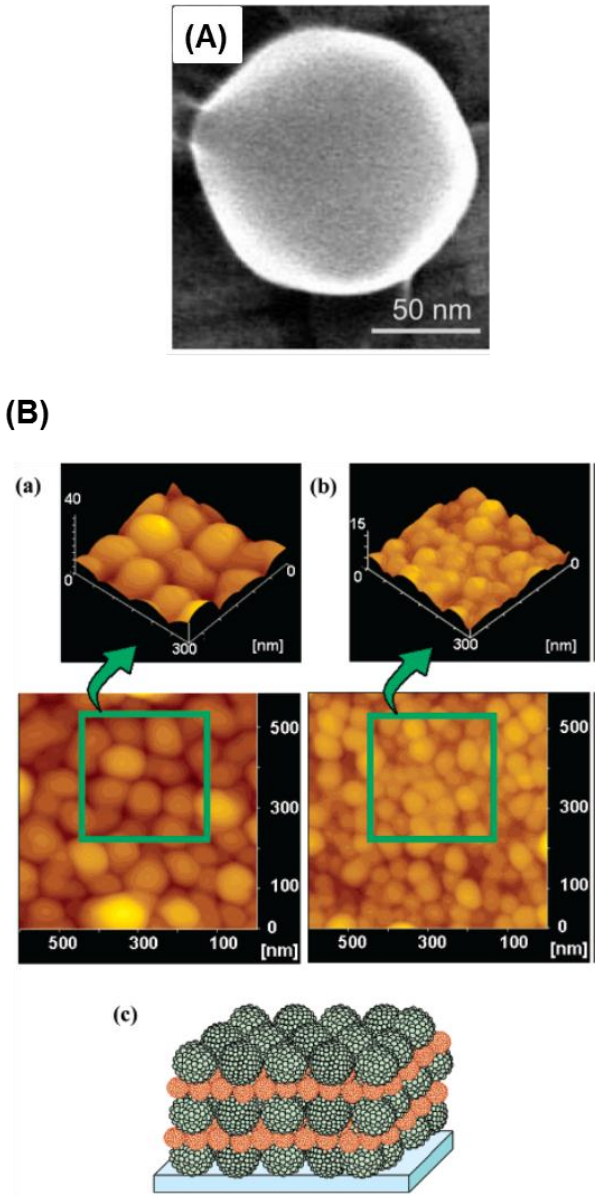

Figure 1-5. (A) SEM image of a cerasome [37]; **(B)** Tapping mode AFM images of the first layer formed with the anionic cerasomes (a) and the second layer formed with the cationic cerasomes (b), and schematic drawing of the three-dimensional assembled structure of the anionic and cationic cerasomes (c) [39].

The maintenance of stable morphology and phase transition behavior makes it possible to employ cerasome as a potential molecular carrier. Previous works in our laboratory reported that the cationic cerasomes can be used as an infusible and cell-friendly gene carrier [40-42] and drug delivery [43]. Moreover, their functions were

enriched further by surface modification. We obtained the magnetic cerasome by covering alloy on its surface [44]. Likewise, the other metal-coated nanohybrid cerasome mobilized by titania, silver, and so on, were also prepared [45, 46].

These achievements illustrated that exploitation of cerasome in the matter of function and application has great potentiality. The cerasome with photoresponsive function has been successively developed using different methods. One method is through intermolecular modification by stable covalent bond, for example, the photoresponsive cerasome derived from cerasome-forming lipids, which contains stimuli-responsive azobenzene functionalized groups **(Figure 1-6)** [47]. Another method is incorporation of cerasome with photodynamic molecules by non-covalent interactions, such as fullerene (C_{70}) [48] and hydrophobic quantum dots (QDs) [49].

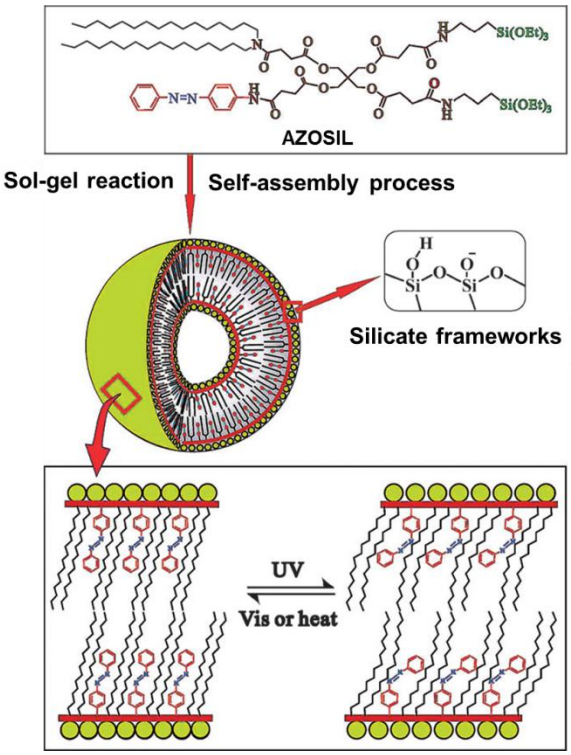

Figure 1-6. Schematic illustration for the formation of photoresponsive cerasome from AZOSIL lipid [47]

1. 4 Purpose of this research

On these grounds, cerasomes have a wide variety of potential as a family of organic-inorganic nanohybrid materials. Application of cerasomes in the research area of electrochemistry is of great importance. However, the potential of cerasome for electroactivity has not been concerned up to the present time. This is my motivation for preparing electroactive cerasome.

In this thesis, I designed and prepared electroactive cerasomes by hybridization with redox active molecules, and developed a novel electroactive nanohybrid system as potent electrochemical interface based on direct electron transfer (DET) (**Figure 1-7**). In this system, naturally occurring enzyme, horseradish peroxidase (HRP), and artificial coenzyme, hydrophobic vitamin B_{12} (HVB_{12}), were utilized as the redox molecules. Moreover, the electrochemical functions of these redox molecules are investigated systematically by electrochemical techniques, such as cyclic voltammetry (CV) and chronoamperometry.

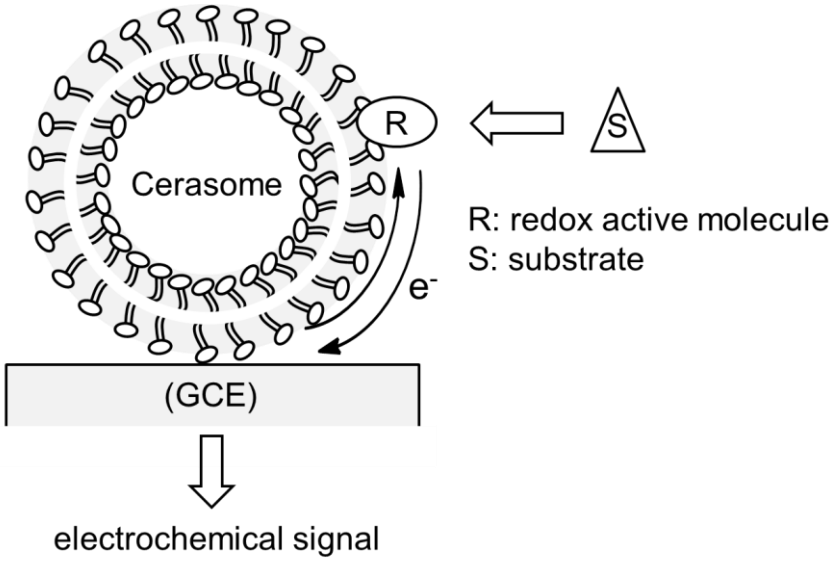

Figure 1-7. Schematic illustration of electrochemical interface formed by cerasome and redox active molecule.

My doctoral thesis is composed of two main parts.

Part 1: Design and characterization of electroactive cerasome modified with redox enzyme

Horseradish peroxidase is an important redox enzyme found in the root of plant horseradish which is used extensively to catalyze the hydrogen peroxide-dependent one-electron oxidation of a wide variety of substrates [50, 51]. Although the root of horseradish contains a number of distinctive peroxidase isoenzymes, the horseradish peroxidase C (HRP) is the primary research subject because it is in high purity and low cost. It is water-soluble enzyme with an isoelectric point close to 8.9 [52]. HRP consists of a hemin prosthetic group embedded in protein. **Figure 1-8 (A)** gives its three-dimensional structure identified by X-ray crystallography. The part colored in red is the heme group. The corresponding chemical structure is shown in **Figure 1-8 (B)**. The resting state of heme-iron is Fe(III), which converses to Fe(II) through accepting electron.

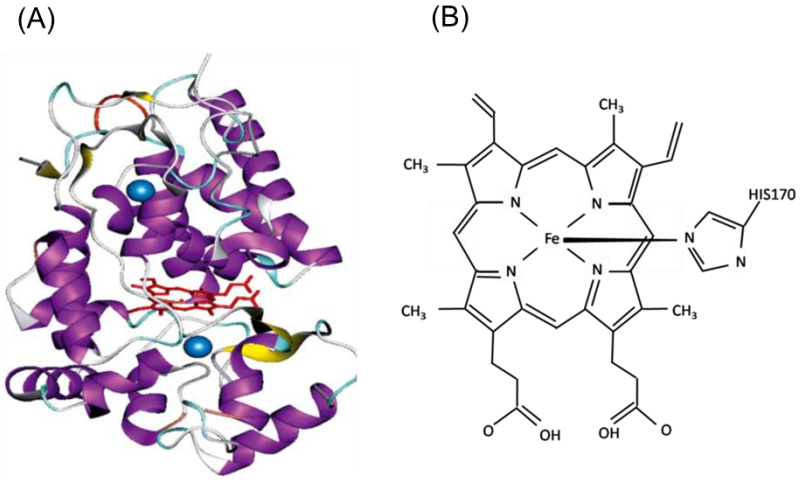

Figure 1-8. (A) Three-dimensional representation of the X-ray crystal structure of HRP and **(B)** the corresponding chemical structure of iron heme group [50].

In this part, an electrochemical interface based on cerasome and HRP was designed

on glassy carbon electrode (GCE). As a reference, liposome and silica nanoparticle (silica NP) were used in place of cerasome because they have partial structures analogous to cerasome. For example, cerasome has the lipid membrane structure like liposome and surface silicate network similar with silica NP. First of all, I systematically compared the structural characteristics of cerasome with its analogues, liposome and silica NP, by means of atomic force microscopy (AFM), scanning electron microscopy (SEM), cryogenic transmission electron microscopy (cyro-TEM) and differential scanning calorimetry (DSC). The results indicated that cerasome combined the merits of liposome with that of NP, such as well biocompatibility induced lipid bilayer structure, and highly structural stability allowing for silicate framework. Furthermore, to clarify the effect of morphological difference among cerasome, liposome and silica NP on electrochemical application, the electrochemical behaviors of immobilized HRP on cerasome/GC were investigated by CV and chronoamperometry.

Part 2: Design and characterization of electroactive cerasome modified with artificial coenzyme

Vitamin B_{12}-dependent enzyme with cobalt species as a catalytic center plays critical roles in various isomerization reactions, which is accompanied by carbon-skeleton rearrangements [53]. In order to simulate the catalytic functions of vitamin B_{12}, hydrophobic vitamin B_{12} (HVB_{12}) derivatives have been developed, which have ester groups in place of the peripheral amide moieties of the natural vitamin B_{12} [54-59]. Herein, I incorporated HVB_{12} (**Chart 1-1**) into lipid bilayer domain of cerasome to form a stable cerasome with well electroactivity. Firstly, I prepared HVB_{12}-cerasome nanohybrid and characterized that HVB_{12} derivative makes stable nanohybrid with with

cerasome by means of UV-vis spectroscopy and differential scanning calorimetry (DSC). AFM measurements were used to observe the morphology of cerasome-HVB_{12} nanohybrid on the solid surface. To examine the electroactive property of the resulting nanohybrid, an electrochemical interface using HVB_{12}-cerasome nanohybrid was fabricated on GCE. The results indicated that cerasome modified with HVB_{12} on the electrode possessed excellent electrocatalytical functions for detecting the various substrates, such as alkyl halide, hydrazine in aqueous solution.

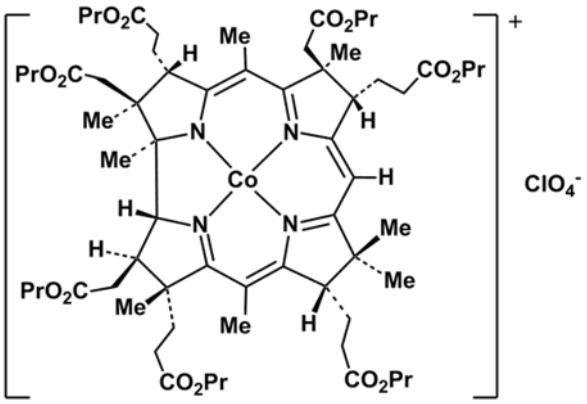

Chart 1-1. Molecular structure of hydrophobic vitamin B_{12}.

1. 5 References

[1] Udeinstein P, Sanchez C. Hybrid organic-inorganic materials: a land of multidisciplinary. J. Mater. Chem. 1996; 4: 511-525.

[2] Itou T, Matsuda H. A SiO_2-ZrO_2 gel film doped with organic pigments made by the sol-gel method for contrast enhancement of color picture tubes. Key Eng. Mater. 1998; 67: 150.

[3] Sanchez C, Soler-Illia G J de A A, Ribot F, Lalot T, Mayer C R, Cabuil V. Designed hybrid organic-inorganic nanocomposites from functional nanobuilding block. Chem. Mater. 2001; 13: 3061-3083.

[4] Chujo Y. Organic-inorganic nano-hybrid materials. Kona 2007; 25: 255-259.

[5] Livage J, Henry M, Sanchez C. Prog. Sol-Gel chemistry of transition metal oxides Solid St. Chem. 1988; 18: 259-341.

[6] Avnir D, Braun S, Lev O, Levy D, Ottolenghi M. in Sol-gel optics, Processing and Applications, ed. By Klein L C, Kluwer Academic Publishers, 1994, pp 539.

[7] Levy D, Avnir D. The effects of the changes in the properties of silica cage along the gel/xerogel transition on the photochromic behaviour of trapped spiropyranes. J. Phys. Chem. 1988; 92: 4734-4738.

[8] Levy D, Einhorn S, Avnir D. Applications of the sol-gel process for the preparation of photochromic information-recording materials: synthesis, properties, mechanisms. J. Non-Cryst. Solids 1989; 113: 137.

[9] Reisfeld R. Prospects of sol-gel technology towards luminescent materials. Opt. Mater. 2001; 16: 1.

[10] Armon R J, Starosvetzky J, Saad I. Sol-gel as reaction matrix for bacterial enzymatic activity. J. Sol-Gel Sci. Technol. 2000; 19: 289.

[11] Peralta-Perez M R, Saucedo-Castaneda G, Gutierrez-Rojas M, Campero A. SiO_2 xerogel: a suitable inert support for microbial growth, J. Sol-Gel Sci. Technol. 2001; 1: 105-110.

[12] http://www.sol-gel.com.

[13] Schöttner G, Kron J, Deichmann K. Industrial Application of hybrid Sol-gel coatings for the decoration of crystal glassware. J. Sol-Gel Sci. Technol. 1998; 13: 183-187.

[14] Aldrich, Fluka, Sigma and Supelco Chiral Products Catalog, 1997, pp 250.

[15] Park H, Kang D, Ahn M, Lee H. Synthesis of organic-inorganic hybrid sols using trifunctional organoalkoxysilanes for dispersion agents. J. Nanosci. Nanotechnol. 2012; 12: 1692-1695.

[16] Stupp S I, Braun P V. Molecular manipulation of microstructures: biomaterials, ceramics, and semiconductors. Science 1997; 227: 1242-1248.

[17] Wen J, Wilkes G L. Organic/inorganic hybrid network materials by the sol-gel approach. Chem. Mater. 1996; 8: 1667-1681.

[18] Avnir D, Braun S, Lev O, Ottolenghi M. Enzymes and other proteins entrapped in sol-gel materials. Chem. Mater. 1994; 6:1605-1614.

[19] Schemidt H. Inorganic-organic composites by sol-gel techniques. Journal of Sol-Gel Science and Technology 1994; 1: 217-231.

[20] Kresge C T, Leonowicz M E, Roth W J，Vartuli J C，Beck J S. Ordered mesoporous molecular sieves synthesized by a liquid-crystal template mechanism. Nature 1992; 359: 710-712.

[21] Vartuli J C, Schmitt K D, Kresge C T, Roth W J, Leonowicz M E, McCullen S B, Hellring S D, Beck J S, Schlenker J L, Olson D H, Sheppardt E. W. Effect of

Surfactant/silica molar ratios on the formation of mesoporous molecular sieves: inorganic mimicry of surfactant liquid-crystal phases and mechanistic implications. Chem. Mater. 1994; 6: 2317-2326.

[22] Dubois M, Gulik-Krzywicki T, Cabane B. Growth of silica polymers in a lamellar mesophase. Langmuir 1993; 9: 673-680.

[23] Hoffmann F, Cornelius M, Morell J, Froba M. Silica-based mesoporous organic-inorganic hybrid material. Angew. Chem. Int. Ed. 2006; 45: 3216-3251.

[24] Huo Q, Margolese D I, Stucky G D. Surfactant control of phases in the synthesis of mesoporous silica-based materials. Chem. Mater. 1996; 8: 1147-1160.

[25] Moreau J J E, Vellutini L, Man M W C, Bied C, Bantignies J L, Dieudonné P, Sauvajol J L. Self-organized hybrid silica with long-range ordered lamellar structure. J. Am. Chem. Soc. 2001; 123: 7957-7958.

[26] Ruiz-Hitzky E, Letaïef S, Prévot V. Novel organic-inorganic mesophases: self-templating synthesis and intratubular swelling. Adv. Mater. 2002; 14: 439-443.

[27] Zhang Q, Ariga K, Okabe A, Aida T. A condensable amphiphile with a cleavable tail as a "lizard" template for the sol-gel synthesis of functionalized mesoporous silica. J. Am. Chem. Soc. 2004; 126: 988-989.

[28] Shimojima A, Kuroda K. Designed synthesis of nanostructured siloxane-organic hybrids from amphiphilic silicon-based precursors. Chem. Rec. 2006; 6: 53-63.

[29] Walcarius, in Encyclopedia of nanoscience and nanotechnology, ed. by Nalwa H S, American Scientific Publishers, Stevenson Ranch, CA 2004, p. 857.

[30] Walcarius A. Electrochemical applications of silica-based organic-inorganic hybrid materials. Chem. Mater. 2001; 13: 3351-3372.

[31] Lin J, Brown C W. Sol-gel glass as a matrix for chemical and biochemical sensing.

Trends Anal. Chem. 1997; 16: 200.

[32] Bescher E, Mackenzie J D. Hybrid organic-inorganic sensors. Mater. Sci. Eng. 1998; C6: 145-154.

[33] Mackenzie J D, Bescher E J. Structures, properties and potential applications of ormosils. Sol-Gel Sci. Technol. 1998; 13: 371.

[34] Katagiri K, Ariga K, Kikuchi J. Preparation of organic-inorganic hybrid vesicle "cerasome" derived from artificial lipid with alkoxysilyl head. Chem. Lett. 1999; 661-662.

[35] Katagiri K, Hashizume M, Ariga K, Terashima T, Kikuchi J. Preparation and characterization of a novel organic-inorganic nanohybrid "cerasome" formed with a liposomal membrane and silicate surface. Chem. Eur. J. 2007; 13: 5272-5281.

[36] Katagiri K, Hashizume M, Ariga K, Kikuchi J. Preparation and surface modification of novel vesicular nano-particle "cerasome" with liposomal bilayer and silicate surface. J. Sol-Gel Sci. Technol. 2003; 26: 393-396.

[37] Kikuchi J, Yasuhara K, in Advances in Biomimetics, ed. by A. George, In Tech, Rijeka, 2011, pp 231-250.

[38] Katagiri K, Hamasaki R, Ariga K, Kikuchi J. Layer-by-layer self-assembling of liposomal nanohybrid "cerasome" on substrates. Langmuir 2002; 18: 6709-6711.

[39] Katagiri K, Hamasaki R, Ariga K, Kikuchi J. Layered paving of vesicular nanoparticles formed with cerasome as a bioinspired organic-inorganic hybrid. J. Am. Chem. Soc. 2002; 124: 7892-7893.

[40] Matsui K, Sando S, Sera T, Aoyama Y, Sasaki Y, Komatsu T, Terashima T, Kikuchi J. Cerasome as an infusible cell-friendly and serum-compatible transfection agent in a viral size. J. Am. Chem. Soc. 2006; 128: 3114-3115.

[41] Sasaki Y, Matsui K, Aoyama Y, Kikuchi J. Cerasome as an infusible and cell-friendly gene carrier: Synthesis of cerasome-forming lipids and transfection using cerasome, Nat. Protocols 2006; 1: 1227-1234.

[42] Tahara K, Moriuchi T, Tsukui M, Hirota A, Maeno T. Ceramic coating of liposomal gene carrier for minimizing toxicity to primary hippocampal neurons. Chem. Lett. 2013; 42: 1265-1267.

[43] Cao Z, Ma Y, Yue X L, Li S Z, Dai Z F, Kikuchi J. Stabilized liposomal nanohybrid cerasomes for drug delivery applications. Chem. Commun. 2010; 46: 5265-5267.

[44] Minamida A, Okada S, Hashizume M, Sasaki Y, Kikuchi J, Hosoito N, Imori T. Creation of magnetic cerasomes through electroless plating and their manipulation using external magnetic fields. J. Sol-Gel Sci. Technol. 2008; 48: 95-101.

[45] Gu F, Hashizume M, Okada S, Sasaki Y, Kikuchi J, Imori T. Metallosomes: artificial cell membranes with ultrathin metallic surfaces derived from cationic cerasomes through electroless plating. J. Ceram. Soc. JPN. 2008; 116: 400-405.

[46] Hashizume M, Yamada M, Katagiri K, Tsuji M, Kikuchi J. Facile functionalization of lipid bilayer vesicles by titania: the use of cerasome-forming lipids for surface and core modification. Bioconjugate Chem. 2006; 17: 1099-1104.

[47] Liang XL, Yue H L, Dai Z F, Kikuchi J. Photoresponsive liposomal nanohybrid cerasomes. Chem. Commun. 2011; 47: 4751-4753.

[48] Ikeda A, Nagano M, Akiyama M, Matsumoto M, Ito S, Mukai M, Hashizume M, Kikuchi J, Katagiri K, Ogawa T, Takeya T. Photodynamic activity of C_{70} caged within surface-cross-linked liposomes. Chem. Asian J. 2009; 4: 199-205.

[49] Li S Z, Ma Y, Yue X L, Cao Z, Liu S Q, Dai Z F. encapsulation of quantum dots inside liposomal hybrid cerasome using a one-pot procedure. J. Dispersion Sci.

Technol. 2010; 31: 1727-1731.

[50] Veitch N C. Horseradish peroxidase: a modern view of a classic enzyme. Phytochemistry 2004; 65: 249-259.

[51] Berglund G I, Carlsson G H, Smith A T, Szöke H, Henriksen A, Hajdu J. The catalytic pathway of horseradish peroxidase at high resolution. Nature 2002; 417: 463-468.

[52] Welinder K G. Amino acid sequence studies of horseradish peroxidase. Eur. J. Biochem. 1979: 96: 483-502.

[53] Lexa D, Saveant J M. The electrochemistry of vitamin B_{12}. Acc. Chem. Res. 1983; 16: 235-243.

[54] Murakami Y, Hisaeda Y, Kajihara A. Hydrophobic vitamin B_{12}. I. Preparation and axial ligation behavior of hydrophobic vitamin B_{12r}. Bull. Chem. Soc. JPN. 1983; 56: 3642-3646.

[55] Murakami Y, Hisaeda Y, Kajihara A, Ohno T. Hydrophobic vitamin B_{12}. II. Coordination geometry and redox behavior of heptamethyl cobyrynate in nonaquaous media. Bull. Chem. Soc. JPN 1984; 57: 405-411.

[56] Murakami Y, Hisaeda Y, Kajihara A, Ohno T. Hydrophobic vitamin B_{12}. III. Incorporation of hydrophobic vitamin B_{12} derivatives into single-compartment vesicles and their alkylation in various molecular aggregates. Bull. Chem. Soc. JPN. 1984; 57: 2091-2097.

[57] Murakami Y, Hisaeda Y, Kikuchi J, Ohno T, Suzuki M, Matsuda Y, Matsu-ura T. Hydrophobic vitamin B_{12}. Part 6. Carbon-skeleton rearrangement via formation of host-guest complexes derived from an ‘octopus’ azaparacyclophane and hydrophobic vitamin B_{12} derivatives: a novel holoenzyme model system. J. Chem.

Soc., Perkin Trans. 1988; 2: 1237-1246.

[58] Murakami Y, Hisaeda Y, Ohno T. Hydrophobic vitamin B_{12}. Part 9. An artificial holoenzyme composed of hydrophobic vitamin B_{12} and synthetic bilayer membrane for carbon-skeleton rearrangements. J. Chem. Soc., Perkin Trans. 1991; 2: 405-416.

[59] Murakami Y, Kikuchi J, Hisaeda Y, Hayashida O. Artificial enzymes. Chem. Rev. 1996; 96: 721-758.

Chapter 2. Design and characterization of electroactive cerasome modified with redox enzyme

2. 1 Introduction

Redox enzymes are one kind of the essential biomolecules participating in a number of biological processes, the most important of which would be the bioenergetics metabolism [1]. The investigation on electrochemical behaviors of redox enzymes is considered as a powerful tool for helping us to understand the metabolic processes and energy conversion in life activities [2-5]. Up to now, great deals of researches on electrochemical studies of redox enzymes have been reported. The studies have focused on the construction of electrochemical interface based on redox enzyme and discussed about their electrochemical functions based on direct electron transfer (DET).

Generally, the simplest redox enzyme can be interpreted as with low molecular weight in the range of 5-20 kDa only taking part in electron convey. From this perspective, the role of HRP with molecular weight of approx. 44000 is analogous to that of some small redox reagent, such as ferrocene participating in displaying reversible or quasi-reversible cyclic voltammetry [6]. However, heterogeneous electrons exchange between immobilized enzyme and electrode surface is not easy to detect by relatively fast techniques, such as cyclic voltammetry. The probable reason is the strong adsorption of enzyme on bare electrode coupled with conformational changes and loss of activity readily induce very low electron transfer rate [6]. As a result, to achieve direct electron transfer, it is of significant importance to seek suitable approaches, for example, enzyme immobilization methods and electrode materials selection. Therefore, it is remarkably worthwhile to develop of biocompatible electrode material for embedding enzyme to realize the direct electron transfer.

Lipid bilayer membranes are assembly of amphiphilic lipids formed spontaneously in water, exhibiting lateral fluidity, surface motility, and self-healing properties [7, 8]. It compromises the basic structural unit of biomembrane, and offers a protein-friendly microenvironment allowing enzyme immobilization without conformational changes. Lipid bilayer membranes participate in information communication and transportation through signals transduction, which play upmost essential role in the process of activity in living organism [9]. It has been widely researched and applied an electrode material to immobilize enzyme due to its merit like natural biomembrane [7, 10, 11].

Nanotechnology is constantly attracted attention, especially in recent years. Its great evolution offers driving force for development of novel biocompatible nanomaterial. As potential matrix, nanomaterials have a lot of merits for fabrication of electrochemical system. On the one hand, nonmaterial provides a biocompatible and inert environment for maintenance of the native structure of the protein. Due to the large surface area, it also supplies more sites for enzyme immobilization [12, 13]. On the other hand, it has been proved that nanoparticles, such as metal nanoparticles, semiconductors can produce a synergic effect among catalytic activity, conductivity and biocompatibility to bring about acceleration of signal transduction in the electrochemical system [14].

A novel nanohybrid material named “cerasome” has been developed recently. It is spontaneously formed by vesicular organoalkoxysilane lipids and contains an inner aqueous compartment exhibiting cell-friendly arising from incorporation of the liposomal architecture and morphologically stable property caused by siloxane framework on the surface [15, 16]. Due to these peculiarly structural and functional characteristics, cerasome has been used for gene and drug delivery, and design of molecular devices [17-23]. Moreover, it has been demonstrated that cerasome can also

serve as an efficient biomaterial for the enzymatic immobilization [22, 23]. For instance, NADH-dependent L-lactate dehydrogenase could be immobilized noncovalently on the cerasome surface with maintenance of catalytic activity [22, 23]. However, as far as we know, there was no report on enzyme immobilization employing cerasome as a matrix for the study of signal transmission.

In this chapter, I associated cerasome composed of cerasome-forming lipids with redox enzymes, HRPs, to fabricate an integrated electrochemical interface. The cerasome not only has the lipid bilayer structure as liposome but also is analogous surface structural characteristics to silica NP derived from tetraethoxysilane (**TEOS**). Therefore, the structural features of it are systematically analyzed in comparison with liposome formed by 1, 2-dimyristoyl-sn-glycero-3-phosphocholine (**DMPC**) and 1, 2-dimyristoyl-sn-glycerol-3-phosphoglycerol (**DMPG**), and silica NP. The results of experiments showed that cerasome coupled the merits of these analogues, thus making the successful achievement of the direct electron transfer of immobilized HRP with electrode surface. During this procedure, cerasome was much superior to traditional liposome and silica NP. Moreover, the transmission of cerasome for catalytic signal of immobilized HRP toward H_2O_2 was investigated in detail.

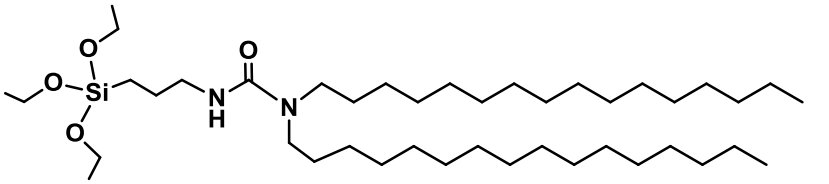

Cerasome forming lipid

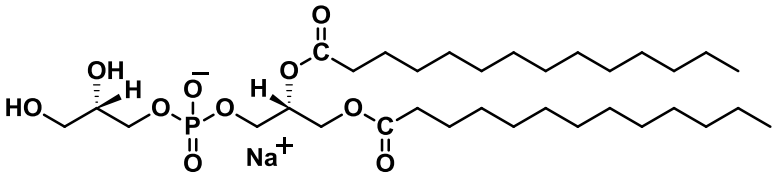

DMPG

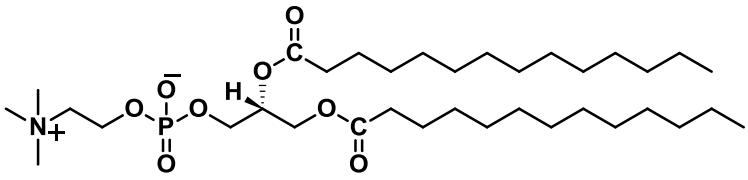

DMPC

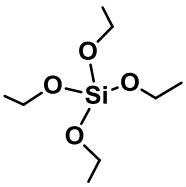

TEOS

Chart 2-1. Chemical structures of the lipids and tetraethoxysilane.

2. 2 Experiments

2. 2. 1 Materials

1, 2-dimyristoyl-sn-glycero-3-phosphocholine (**DMPC**; ≥99%), 1, 2-dimyristoyl-sn-glycerol-3-phosphoglycerol (**DMPG**; ≥99%), Horseradish peroxidase (**HRP**; Mw≈ 44000) were purchased from Sigma-Aldrich. Ethanol (99.9%) and tetraethoxysilane (**TEOS**) were obtained from Wako pure chemical industry and Shin-Etsu Chemical Co., Ltd, respectively. All the chemicals were utilized as-received state without any further treatments. Ultra-pure water (18.3 MΩ·cm) used in all experiments was prepared with Milli-Q Labo. Dihexadecylamine was prepared by the reaction of n-hexadecylamine with 1-bromohexadecane in the presence of sodium carbonate in ethanol.

2. 2. 2 Syntheses

The cerasome-forming lipid, *N*, *N*-dihxadecyl-*N*'-[3-(triethoxysilyl)propyl]urea was synthesized from 3-(triethoxysilyl)propyl isocyanate and *N*, *N*-dihxadecylamine in our laboratory according to the report [16] (**Scheme 2-1**).

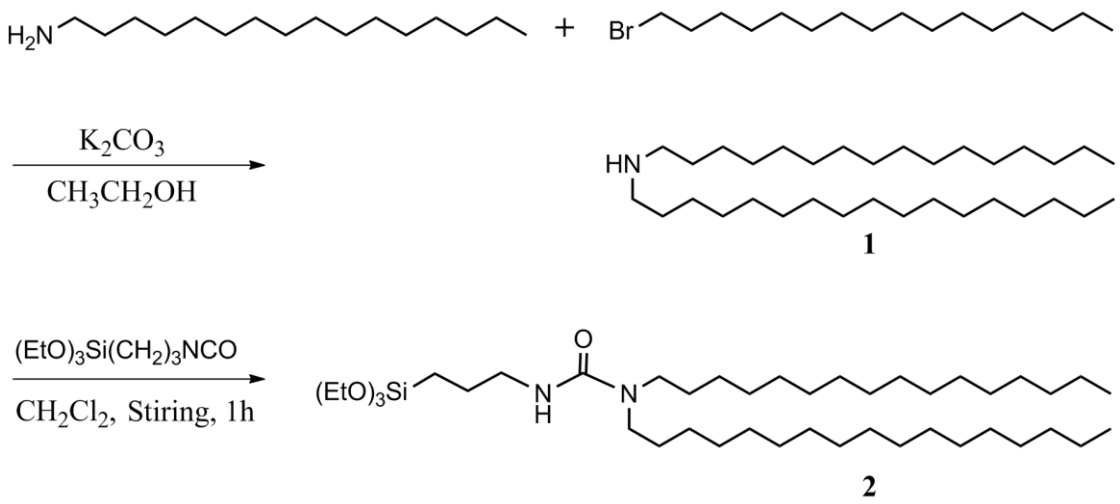

Scheme 2-1. Synthesis of cerasome-forming lipid.

Synthesis of *N, N*-dihexadecylamine (Product 1)

To a solution of n-hexadecylamine (50 g, 0.21 mol) in 100 ml of ethanol were added 1-bromohexadecane (30 g, 0.16 mol) and potassium carbonate (45.02 g, 0.32 mol) in turn in a round bottom flask equipped with reflux condenser and a magnetic stirrer. The hot mixture was then filtered after being reflux for 120 h. The solvent was removed by rotary vacuum evaporator at 35 °C, and then the crude product was dried *in vacuo*. The precipitates were then purified by recrystallization from hexane to produce a colorless power. The yield is 15.2 g (32 %); R_f = 0.35 (silica gel 60F254 plate Merck, chloroform-methanol, 9:1 v/v) ^{1}H-NMR (400 MHz, $CDCl_3$, TMS): δ 0.88 [6H, t, *J* = 6.8 Hz, $NCH_2CH_2(CH_2)_{13}CH_3$], 1.25-1.30 [52H, m, $NCH_2CH_2(CH_2)_{13}CH_3$], 1.45 [4H, m, $NCH_2CH_2(CH_2)_{13}CH_3$], 2.57 [4H, t, *J* = 6.8 $NCH_2CH_2(CH_2)_{13}CH_3$].

Synthesis of *N,N*-dihxadecyl-*N'*-[3-(triethoxysilyl)propyl]urea (Product 2)

0.33 g (1.29 mmol) of 3-(triethoxysilyl)propyl isocyanate was added into dihexadecylamine (0.50 g, 1.07 mmol) in 30 ml of dry dichloromethane. The mixture was stirred for 2 h under N_2 atmosphere at room temperature. After that, the solvent was removed under reduced pressure to get colorless oil. The crude product was purified by chromatography (silica gel, Wako gel C-300) with hexane-ethyl acetate (4:1 v/v) as an eluent. The yield was 680 mg (78 %); R_f = 0.2 [silica gel 60F254 plate Merck, hexane-ethyl acetate (4:1, v/v)] ^{1}H-NMR (400 MHz, $CDCl_3$, TMS): δ 0.63 [2H, t, *J* = 8.1 Hz, $SiCH_2$], 0.88 [6H, t, *J* = 6.8 Hz, CH_3], 1.16-1.33 [61H, m, J_1 = 7.0, J_2 = 7.0 Hz, $(CH_2)_{13}CH_3$, OCH_2CH_3], 1.51-1.65 [4H, m, NCH_2CH_2, $SiCH_2CH_2$,], 3.14 [4H, t, *J* = 7.6 $NHCH_2$], 3.23 [2H, t, *J* = 6.5 Hz, CH_2NHCO], 3.81 [6H, q, *J* = 7.0 Hz, OCH_2CH_3], 4.43 [1H, br, *J* = 5.6 Hz, NHCON];

2. 2. 3 Preparation of silica nanoparticle

The monodispersed silica nanoparticles ca. 225 nm in diameter was synthesized by hydrolysis of TEOS in the presence of sodium dodecyl sulfate (SDS) as a dispersant [24]. Firstly, SDS was dissolved in 0.5 M NH_4OH aqueous solution, and TEOS were diluted separately with the same amount of ethanol. TEOS/H_2O/EtOH were controlled at 0.2/10/10 in molar ratio. The amount of SDS was fixed to be 0.2 % in weight percentage versus the total weight of sols (70 g). The as-prepared silica NPs were carefully rinsed with ethanol, and then dried under vacuum to remove the dispersant.

2. 2. 4 Preparation of liposome

Binary large unilamellar vesicles (LUV) liposome was prepared by hydration of a mixture lipid film (DMPC/DMPG, 7:3 mole/mole). Firstly, neutrally charged DMPC stock solution in dry chloroform (10 mM) and negatively charged DMPG stock solution in dry chloroform/methanol (9:1 v/v, 10 mM) were dried under vacuum for 4 h to obtained the thin lipid film. Then the film on the wall of vial was hydrated with an appropriate amount of Milli-Q water at 40 ℃. The liposome dispersion was extruded through two stacked polycarbonate membrane (200 nm in the pore diameter) for 21cycles followed by five freeze-thaw cycles (-196 ℃ and 50 ℃).

2. 2. 5 Preparation of anionic cerasome by ethanol sol injection method

Due to the poor water solubility of cerasome-forming lipid (**Chart 2-1**), cerasome was prepared by ethanol sol injection method as the previous report in our group [20]. Firstly, cerasome-forming lipids were hydrolyzed in the mixing solution of H_2O, HCl, and EtOH, which molar ratio was controlled at 1: 19: 0.03: 200 (cerasome-forming lipid: H_2O: HCl: EtOH), for 12 h at room temperature by using the votex microtiter.

Then 6 μL of the above solution was injected into 1 mL of MilliQ water at 40 °C under stirring followed ten freeze-thaw cycles (-196 °C and 50 °C). The final concentration of lipids was fixed at 0.5 mM. The dispersions of cerasomes were incubated at 40 °C overnight before use to develop their surface siloxane networks.

2. 2. 6 Fabrication of enzyme modified electrode

A glassy carbon electrode (**GCE**) electrode with a diameter of 3 mm was firstly polished on polishing cloth with 0.05 μm alumina powder, and then rinsed with deionized water followed by sonication in Milli-Q water, and then dried with nitrogen stream. 5 μL of the prepared cerasome aqueous dispersions (0.5 mM) were cast on the surface of pretreated GCE. The cerasomes were deposited on the surface of electrode after water evaporated slowly. Then 5 μL of HRP solutions (5 mg/ml, in 0.1 M citrate buffer pH 5.6) were dropped on the surface of the cerasome modified electrode. The final mole ratio of cerasome-forming lipids to HRPs on the electrode surface is controlled at 100: 23. The HRP/cerasome/GCE modified electrode was obtained after evaporation of water. The above modified electrode was stored in refrigerator at 4 °C overnight and rinsed with Milli-Q water before electrochemical measurement to remove excess of HRPs on the electrode surface.

The procedure of construction of reference modified electrodes, silica NPs/GCE and liposome/GCE, are the same with the cerasome/GCE. Briefly, 5 μL of fresh silica NPs and liposomes aqueous dispersion were cast on pretreated GCE, and dried slowly at room temperature. The HRP/liposome/GCE and HRP/silica NP/GCE were fabricated also using the same procedures as above.

2. 2. 7 Measurements

The morphological structure of samples were analyzed by a scanning electron microscope (**SEM**, JEOL，JSM-7400F) operating at 5 kV, atomic force microscopy (**AFM**, SPI3800N) and cryogenic transmission electron microscopy (**cyro-TEM**, JEOL JEM-3100 FEF). For the SEM measurements, samples were prepared by casting on the aluminum foil. The samples for AFM were prepared by simple cast method on the freshly cleaved mica surface and the images were obtained in the tapping mode in ambient atmosphere.

Circular dichrosim (**CD**) experiments were carried out with a Jasco-spectropolarimeter (J-820) at room temperature in a quartz cuvette with a 1 mm path length. Each spectrum was obtained scanning 3 times at 0.5 nm intervals with the scan rate of 20 nm/min. The concentration of HRPs was fixed at 0.2 mg/ml. UV-vis spectra were collected using UV-vis spectrophotometer (Jasco, V-670).

Differential scanning calorimetry (**DSC**) was conducted using a VP-DSC micro-calorimeter (MicroCal LLC) with the heating rate of 0.5 °C/min. In the case of vesicular sample the phase transition temperature (T_m) and enthalpy change for the transition (ΔH) were obtained from thermograms.

Electrochemical measurements were performed on CHI 630d electrochemical workstation at room temperature by cyclic voltammetry (**CV**) and chronoamperometry. All the electrochemical experiments were carried out with the three-electrode cell composed by a HRP immobilized GCE electrode as working electrode, an Ag/AgCl (saturated KCl) as reference electrode and platinum wire as an auxiliary electrode. Citrate buffer solution (0.1 M, pH 5.6) containing 0.1 M KCl prepared with citric acid and sodium citrate was used as electrolyte. All experimental buffer solutions were

purged with highly purified nitrogen for at least 30 min prior to the beginning of experiments to remove the dissolved oxygen, and nitrogen atmosphere was maintained during electrochemical measurements.

2. 3 Results and discussion

2. 3. 1 Construction of enzyme modified electrode

Considering the affection of surface charge on electrochemical experiments, an anionic urea-type cerasome was selected, which was derived from organoalkoxysilane lipid (**Chart 2-1**). As a control, a negatively charged liposome formed from binary lipids (DMPC/DMPG) shown in **Chart 2-1** were utilized in this research. Since silica NP had spherical morphology and surface chemical structure, such as hydroxyl group, resembling to that of cerasome, it was also used as counterpoint. In this work, HRP was absorbed onto cerasome, silica NPs, and liposome modified electrode.

Scheme 2-2 shows the overall schematic diagram of the self-assemble procedure of electrochemical interface. Three types of modified electrode based on various matrixes were firstly fabricated by simple casting method, and then HRPs were assembled on modified electrode surface through electrostatic interaction. The zeta-potential of liposome, silica nanoparticle and cerasome are negative, at -30.3, -43.7 and -37.1 mV in ascorbic acid buffer solution with pH 5.6, respectively (**Table 2-1**). Thus, the cleaning glassy carbon electrode surfaces are negatively charged after treated with cerasome, liposome and silica NP dispersion. As previous report, the morphological stability of conventional liposome formed by phospholipids is relatively low. Thereby, it easily loses the vesicular structure and flattens as the water evaporate, giving rise to planar bilayer membrane. However, cerasome exhibits higher morphological stability than liposome due to the presence of ceramic-like structure on the lipid bilayer, so that it can maintain its initial structure even in dry state. For this reason, I speculate that finally, both cerasome and silica NP can keep their original state on HRP/cerasome/GCE and

HRP/silica NP/GCE modified electrode, whereas, liposome becomes multi-wall planar bilayer membrane on electrode. The following results of morphological characterization give powerful supports to this speculation. HRP molecule has positive charge when it is dispersed in the aqueous medium with pH 5.6 under the isoelectric point (Ip $\approx$ 8.9) [25]. Thus, in the following step, HRP molecule in the citrate buffer solution (pH 5.6) can adhere well to the above as-prepared modified electrode surface by electrostatic interaction.

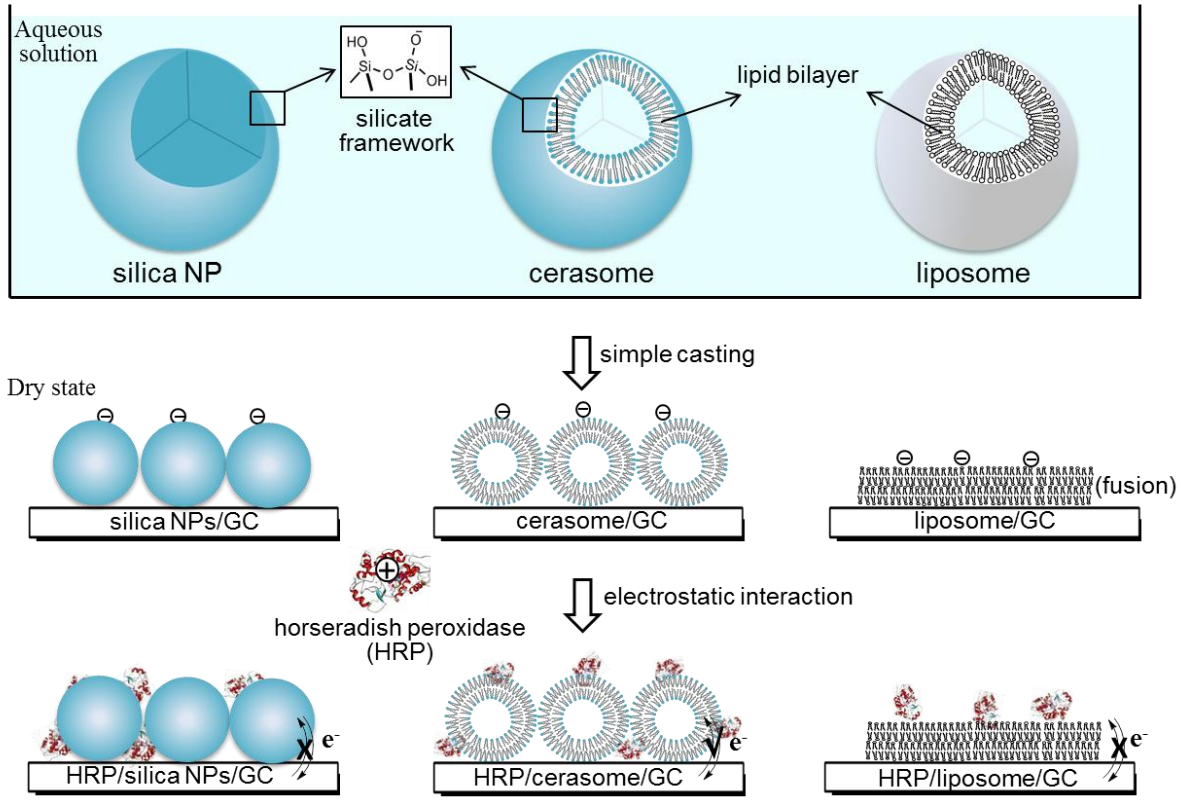

Scheme 2-2. Schematic illustration of procedure of various modified electrode fabrication.

Table 2-1. Zeta potential and size distribution of cerasome, silica NP and liposome in citrate buffer solution (pH, 5.6) at 25 °C.

	Cerasome	Silica NP	Liposome
Zeta potential / mV	-30.3	-43.7[a]	-37.1
Size / nm (PDI)	213(0.152)	225(0.049)	181(0.25)

a. Zeta potential measurement of silica NP was performed in citrate buffer solution containing 10% ethanol in volume to prevent the aggregation.

2. 3. 2 Characterization of hybrid nanomaterials

2. 3. 2. 1 Investigation of universality of hybrid nanomaterials

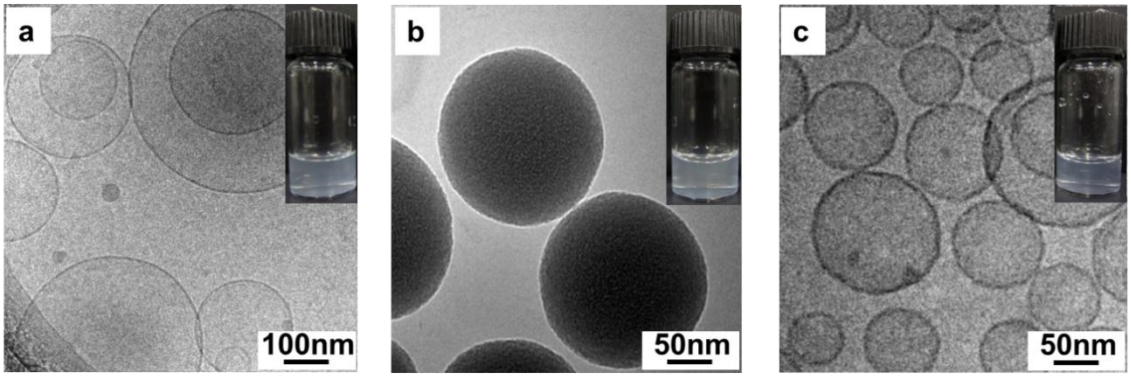

Figure 2-1. The cryo-TEM micrographs of cerasome (a), silica NP (b) and liposome (c) in Milli-Q water. [DMPC/DMPG] = 2 mM, [cerasome forming lipid] = 3.5 mM and [silica NP] = 3.5 mg/ml. **Inset:** corresponding photographs in aqueous solution.

Cryo-TEM is used to elucidate the morphology because it can offer the actually structural information of object composed by hydrophilic molecule in aqueous solution. Moreover, in contrast to classic TEM, the principle advantage of cryo-TEM is capable of maintaining specimens in their native, hydrated states [26-28]. **Figure 2-1** shows the cryo-TEM images of cerasomes (a), silica NPs (b) and liposomes (c) dispersed in Milli-Q water. According to the cryo-TEM images, silica NPs have spherical shape with a rough surface in common with published work [29]. The silica NPs are ca. 220 nm in

diameter, as confirmed by TEM. It is closed to hydrodynamic mean size, 225 nm determined by DLS method (**Table 2-1**), revealing a very narrow size distribution. The vesicular structure of liposome is also identified by cryo-TEM. It is clearly seen the circle shape and inner aqueous compartment from **Figure 2-1(b)**, which are found to be consistent with the reported vesicular feature of liposome [28]. In the same condition, the cryo-TEM image of cerasome also displays the typical vesicular morphology similar with that of liposome but different with that of silica NP. No aggregates are formed from the results of cryo-TEM, demonstrating that all of species have excellent dispersion in aqueous solution. The high zeta-potential values of all species afford them well dispersion in water and formation of a light turbid homogeneous solution (**Inset of Figure 2-1)**. These indicate that cerasome, silica NP and liposome have similar surface property, namely, well water solubility, which is significant for serving as biomaterial.

The results of TEM results show that cerasome, silica NP and liposome have different morphologies in aqueous solution. By comparison, only the cerasome and liposome possess lipid bilayer membrane. The phase transition from gel to liquid-crystalline is one of remarkable characteristics for vesicle molecular assembly system [30]. **Figure 2-2** presents the DSC thermographs of cerasome (a), silica NP (b) and liposome (c), respectively. Liposome gives a pre-transition at 14 ℃ and the main chain-melting transition (T_m) at 24.6 ℃ from curve c. The T_m is 30 ℃ for cerasome, which definitely indicates it still maintains the intrinsic feature structure of the conventional liposome, even though with the modification of siloxane group on the surface. By contrast, nearly no observation of exothermic or endothermic peaks for silica NP illustrates there is no phase transition behavior to occur, suggesting that silica

NP does not have the structure of lipid bilayer membrane.

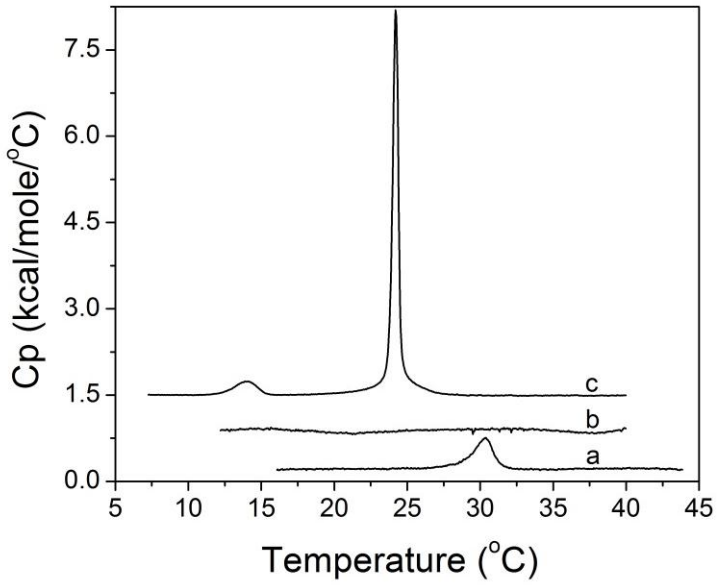

Figure 2-2. DSC thermogram of cerasome (a), silica NP (b), and liposome (c) in aqueous solution at a scan rate of 30 °C/h. [cerasome forming lipid] = 1 mM, [DMPC/DMPG] = 1 mM and [silica NP] = 1 mg/ml.

2. 3. 2. 2 Morphological differences characterized by SEM and AFM

Differing from cryo-TEM, which can provide the state of cerasome, liposome and silica NP in aqueous solution, SEM is capable of offering the surface morphology of samples in dry state. **Figure 2-3** display the SEM images of cerasome (a), silica NP (b) and liposome (c) deposited on aluminum foil. According to the SEM images, obvious globular morphology can be visualized for cerasome as well as silica NP because of the presence of siloxane network on the surface. However, under the same condition conventional liposome formed with phospholipids cannot be observed initial spherical structure in aqueous solution because it cannot maintain vesicular structure due to poor structural integrity.

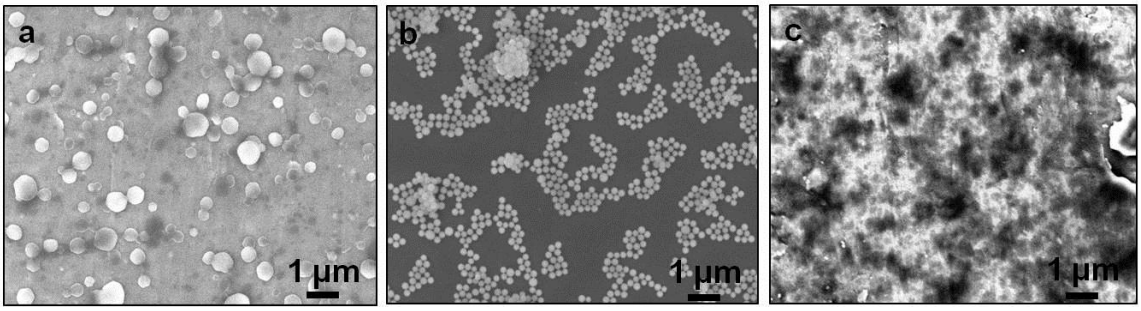

Figure 2-3. Representative SEM images of cerasome (a), silica NP (b) and liposome (c) on aluminum foil.

To further observe surface morphologies, the AFM is then employed because it can map out the 3D topography, height and roughness of species at normal pressure. Based on the AFM images of cerasome (a), silica NP (b) and liposome (c), the substrate shows nearly flatten surface for liposome, but the morphology with globular features for silica NP and cerasome (**Figure 2-4**). These indicate that both cerasomes and silica NPs are able to retain their as-prepared morphologies due to the presence of siloxane network. Whereas, as a result of destroyed spherical structure after evaporation of solvent, a typically stepped surface on the mica deposited by liposome is observed. The height of each step is about 5 nm measured from the height profile line, which is in agreement with the thickness of the single-layer DMPC bilayer, 5.3 nm, determined by X-ray [31]. It can be demonstrated that planar membrane formed on substrate from the fusion of liposome vesicle. However, cerasome similar to silica NP has the ceramic-like surface, imparting it highly mechanical strength. As a result, cerasome can keep same morphology in both aqueous solution and dry solid substrate surface.

For these reasons, cerasome could be utilized as a nanomaterial for enzymatic immobilization even in dry state. In conclusion, as the new artificial cell, cerasome overcomes the morphological stability limitation of the traditional liposome, which

makes it possible to be practically applied in biosensor and other fields.

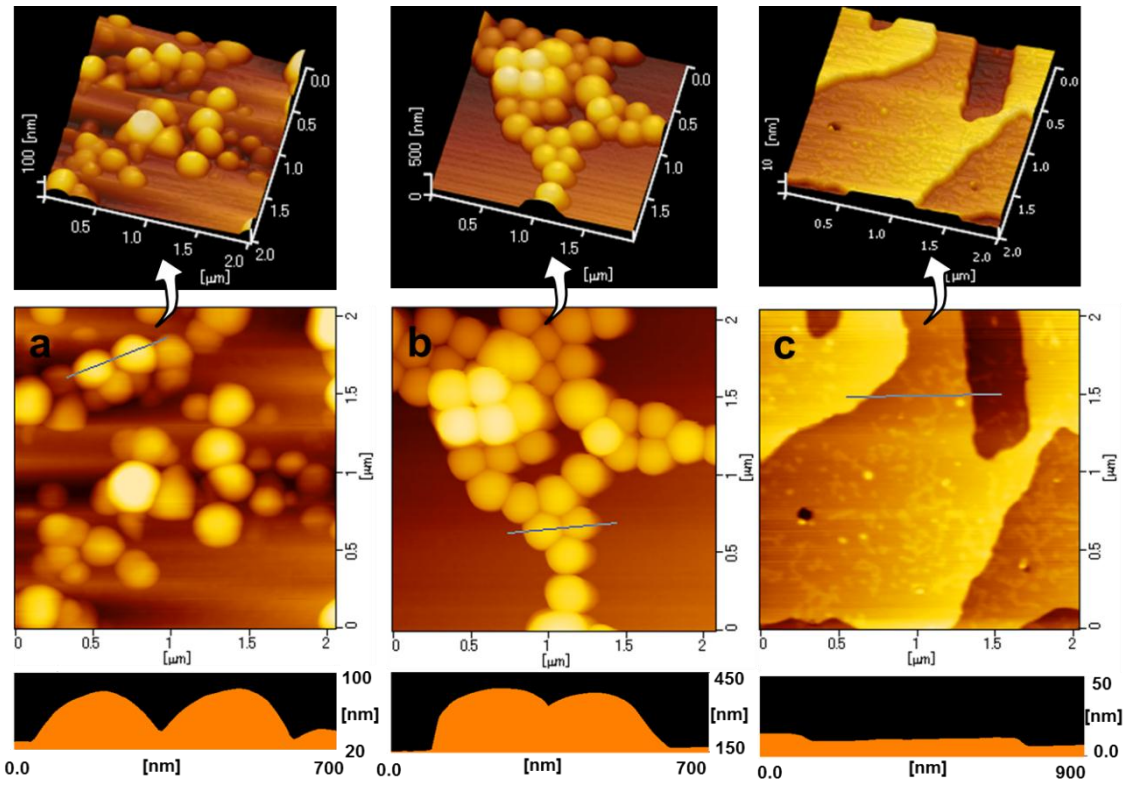

Figure 2-4. Tapping mode AFM images and corresponding profile line for cerasome (a), silica NP (b) and liposome (c) on fresh mica. The simple casting method was utilized in this experience.

2. 3. 3 Conformational studies of immobilized enzyme

Considering the specific structure of cerasome, it was used for immobilization of enzyme. In order to evaluate the possible denaturation of heme proteins during the process of immobilization, UV-vis spectroscopy was utilized to monitor the whole immobilization process by providing the information of the Soret band changes [32]. For the immobilized HRP onto the cerasome, the Soret band is located at 404 nm in the spectrum of HRP/cerasome, showing slight red-shift comparing to the free HRP with a strong absorbance at 403 nm (**Figure 2-5**). These results illustrate that there is non-pronounced fundamental changes of miro-environment of HRP, that is to say, the

native structure of HRP maintained during the procedure of immobilization on cerasome.

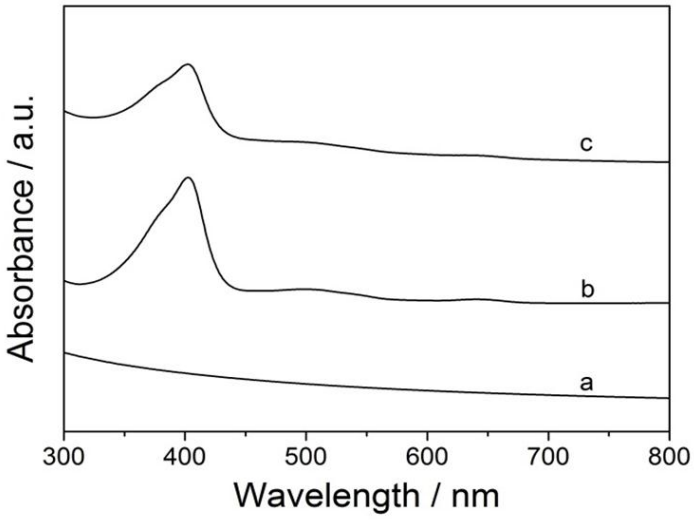

Figure 2-5. UV-vis absorption spectra of cerasome (a), HRP (b) and HRP/cerasome (c) in citrate buffer solution of pH 5.6.

Circular dichroism spectroscopy has been proved to be quite sensitive for the changes of polypeptide backbone conformations, especially secondary and tertiary structure. **Figure 2-6** shows CD spectra of 0.2 mg/ml HRP in the citrate buffer solution (pH 5.6) with and without cerasome in the wavelength region at the far-UV **(A)** and Soret region **(B)**. **Figure 2-6(A)** shows the characteristic CD spectrum of α-helix structure of enzyme, on which there is an positive band at 192 nm corresponded to the π-π* transition of the amide groups in peptide chain of HRP and two distinct negative absorption bands of the π-π* and n-π* amide transition of peptide chain at around 207 and 223 nm, respectively, [33]. The conformational changes upon adsorption of HRPs on cerasome are not significant, indicating that the native secondary structure of HRP retain well in the presence of cerasome.

The CD spectra of heme protein in the Soret region can response to the integrity of

the heme crevice [34]. Heme is CD inactive in its free state but it becomes CD-active in an asymmetric environment of a protein [35, 36]. The CD spectra in Soret region of free HRP and HRP/cerasome are shown in **Figure 2-6(B)**. By comparison, there are no clearly observed changes of CD spectra in Soret region, suggesting the heme does not remove from the HRP, and the tertiary structure of HRP is not obviously destroyed after adsorption on the cerasome.

Base on the above results, it is estimated that cerasome could possess the superior biocompatible properties, which may offer a moiety and mild condition beneficial for maintenance of enzyme bioactivity.

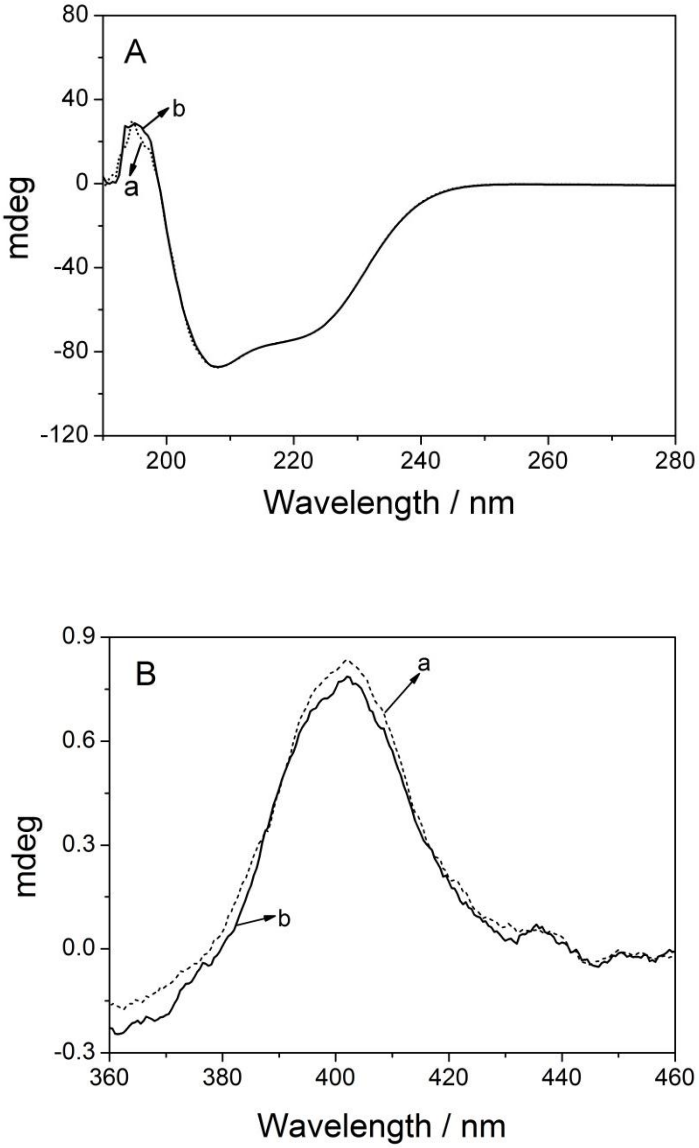

Figure 2-6. CD spectra of free HRP (a) and HRP/cerasome (b) in the region of far-UV **(A)** and the Soret region **(B)** in citrate buffer solution (pH 5.6) at room temperature.

2. 3. 4 Electrochemical properties of enzyme modified electrodes

To further prove the influence of electrode materials with different structures on the electron transfer of immobilized enzyme, I investigated the electrochemical response of various modified electrode at room temperature (ca. 25 °C). From the DSC thermorgrams (**Figure 2-2**), the phase transition temperature T_m of cerasomes is about

30 °C. So the measurement temperature is below T_m. However, the HRP molecules are adhered on the surface of cerasome, not embedded in the lipid bilayer membrane. As a result, the electrochemical behaviors of HRP molecules are not obviously affected by the state of lipid bilayer. For this reason, the experimental temperature possibly exerts a very weak influence on the electrochemical response of immobilized HRP.

First of all, the electrochemical behaviors of various modified electrodes without HRP were investigated in oxygen-free citrate buffer solution at the scan rate of 200 mVs^{-1} using CV. No obvious redox peaks are observed on cerasome/GCE, liposome/GCE, silica NP/GCE and bare GCE in **Figure 2-7 (A)**. These suggest cerasome, liposome, silica NP, and GCE are electroinactive in the potential window. After introduction of HRP molecules, only very weak electrochemical signals can be seen on the HRP/bare GCE, because the direct electron transfer between the enzyme and bare electrode is usually hard to achieve. There are several factors: 1) the electroactive center of enzyme is deeply buried inside the polypeptide chains, which inhibits the electron exchange of enzyme with electrode; 2) the adsorption of macromolecular impurities or denatured enzymes on electrode surface may prevent the electron transfer between proteins and electrode; 3) unfavorable orientations of enzyme also probably increase the distance between the redox center and electrode, which is not beneficial for the electron exchange between enzyme and electrode [37].

There is no clear redox peaks can be observed on the HRP/liposome/GCE and HRP/silica NP/GCE. However, remarkable voltammetric responses for HRP/cerasome/GCE are obtained, ascribing to the direct electron transfer for the heme-Fe^{III}/Fe^{II} couples. The anodic peak potential (E_{pa}) and cathodic peak potential (E_{pc}) of the HRP/cerasome/GCE are located at -0.11 and -0.23 V, respectively. The formal

potential (E_p, calculated from the average of E_{pa} and E_{pc}) is around -0.17 V, which has just a slightly negative shift compared with the reported value of -0.16 V [38]. These observations indicate that the immobilized cerasomes on electrode surface are helpful for HRPs to take their suitable orientation toward electrodes and decrease the distance between the redox center of HRP and electrode surface. Additionally, cerasome can provide the microenvironment for maintenance of enzyme activity. As a result, it can efficiently enhance the enzyme electron transfer.

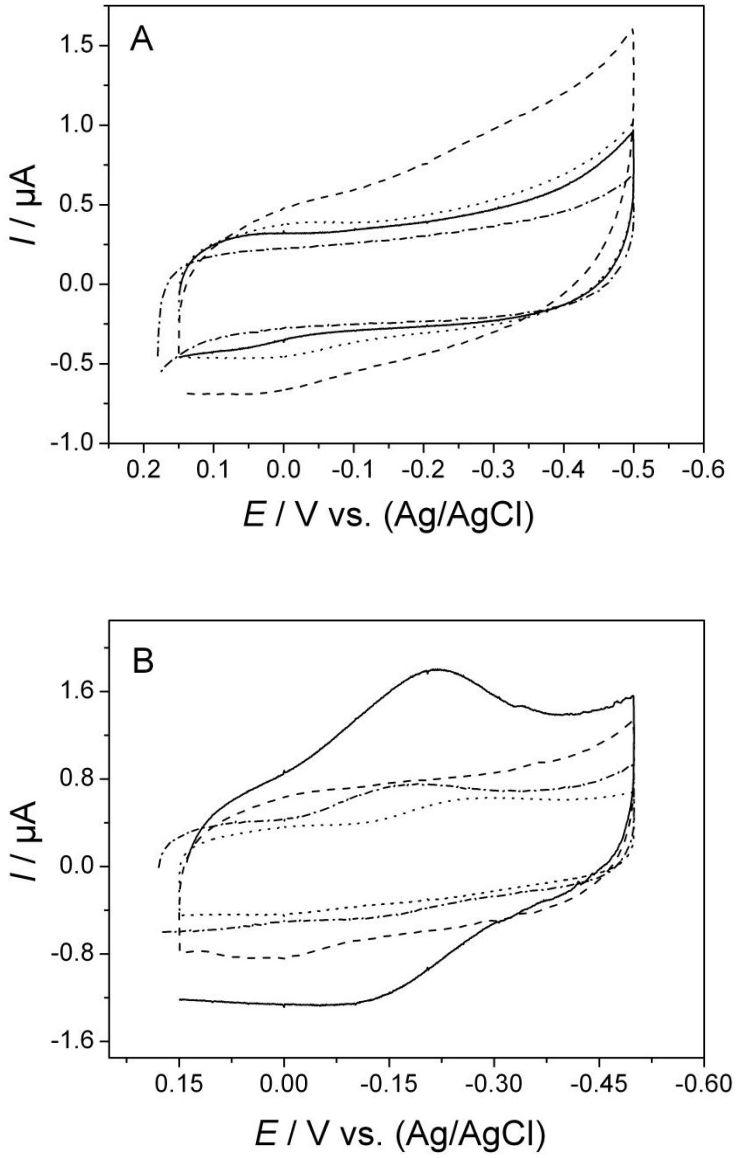

Figure 2-7. CVs of cerasome/GCE (solid), liposome/GCE (dash), silica NP/GCE (dot) and bare CGE (dash-dot) modified electrodes in oxygen-free 0.1 M citrate buffer solution (pH 5.6) without **(A)** and with **(B)** HRP. Scan rate, 200 mV s^{-1}.

On the HRP/liposome/GCE modified electrode, no obviously signal wave can be observed. It is possible that the electron transfer from the enzyme to electrode is blocked by planer membrane film formed on the surface of GCE due to the fusion of liposomes. The previous work has proved that the traditional liposome dispersion on the

solid surface became flatten multi-layer membrane-like films while they were dried [8, 37]. The results of AFM and SEM for liposome in my research also definitely clarified that stock of bilayer membrane formed on the solid surface.

According to the theoretical model established by Marcus theory, the factors affect the rate of electron transfer (ET) include driving force arising from potential difference between electron donor and electron acceptor, the reorganization energy, which qualitatively reflects the structural rigidity of the redox species, and the distance between the two redox centers [39-41]. Theories and experiments predict that the rate of electron transfer (K_{ET}) decreases exponentially with the distance of the involved redox centers, when the distance is substantially over atomic dimensions (＞0.3 nm) [42]. The rate equation of ET can be estimated as follow: [42]

$$k_{ET} = 10^{13} e^{-\beta(d-3)} e^{-(\Delta G^0 + \lambda)^2 / 4RT\lambda}$$

β, constant for a given electron donor/acceptor pair in a defined medium

d, distance between the donor and the acceptor

$-\Delta G^o$, driving energy

λ, Marcus reorganization energy

According above equation, generally, electron transfer distance with a fast, moderately oxidizing relay is calculated to be ca. 2 nm [42]. However, the thickness of planar membrane in my experiment is ca. 5 nm, much larger than the effective electron transfer distance. It prevents the electron exchange of immobilized HRP molecule with electrode surface. Consequently, there are nearly no voltammetric waves on HRP/liposome/GCE modified electrode in **Figure 2-7 (B)**.

On the CV of HRP/silica NP/GCE, only a very weak cathodic peak can be observed.

The possible explanation for this phenomenon is that the immobilized HRP molecules go through the structural changes, which cause the loss of function and activity. The enzymatic structure and activity is intensely dependent on the size of silica NP [43]. The smaller nanoparticles are more favorable to maintain the native structure and intrinsic activity of enzyme compared to the larger nanoparticles [43]. Geometrically, the surface curvature of silica NP decreases when the size of silica NPs increases. The edges of the binding protein molecule are at a shorter distance from the surface of silica NP with large size, giving rise to a stronger interaction between the enzyme and silica NP [43]. In my experiment, the silica NP (dia. 225 nm) with small surface curvature probably induces in significant structural changes of enzyme. However, in case of cerasome the introduction of lipid bilayers remarkably reduces the inherent high rigidity and mass density in comparison with silica NP, and enhances the biocompatibility [44, 45]. As a result, cerasome is capable to supply more beneficial condition for maintenances of HRP bioactivity compared to silica NP [44, 45].

Figure 2-8 (A) gives the typical CVs of HRP/cerasome/GCE modified electrode at different scan rates. It is clear that both cathodic peak and anodic peak currents varies linearly with the scan rates in the range of 100-700 mV s^{-1} as shown in **Figure 2-8 (B)**. The linear regression equations are $y = 6.477 x + 0.43$ ($R^2 = 0.9979$, n=7) for cathodic peaks and $y = -5.788 x - 0.0749$ ($R^2 = 0.9932$, n=7) for anodic peaks. This suggests a typical surface-controlled electrode process on the HRP/cerasome/GCE modified electrodes [46]. According to Faraday's law, $Q = nFA\Gamma^*$ (where F is the Faraday constant and Γ^* represents the surface concentration of electroactive HRP, Q can be calculated by integrating the reduction peak of HRP, n stands for the number of electrons transferred, and A represents the area of the electrode surface, here using the

geometric area of the GC electrode (0.07 cm^2)), the surface concentration of electroactive HRP (Γ^*) at HRP/cerasome/GCE electrode was calculated to be 1.2×10^{-11} mol cm^{-2}. The value is a little lower than theoretical monolayer coverage for HRP, about 2.0×10^{-11} mol cm^{-2} [47], indicating that HRP possibly has an unsaturated monolayer adsorption on cerasome surface.

The amount of electroactive HRP was calculated to be 8.4×10^{-13}mol, based on the surface concentration of electroactive HRP on electrode surface. In my experiment, 5 μL of HRP solution (5 mg/ml, $M_w\approx44000$) were cast on the electrode surface. So the amount of deposited HRPs on electrode was 5.0×10^{-10} mol. Thus the percentage of electroactive HRP molecules among total deposited proteins on the glassy carbon electrode was calculated to be 0.17 %. From this result, it is noted that a large proportion of the HRP molecules cannot exchange electron with electrode. It is probable that on one hand, some amount of HRP molecules were lost during preparation of modified electrode; on the other hand, the HRP molecules far from the electrode surface were hard to achieve the electron transfer with electrode due to rather long distance. Eventhough the surface of cerasome is completely covered by HRP molecules in ideal situation according to the results of following calculation, the distance between two electroactive centers of HRP is rather longer than the critical point, 2 nm. Therefore, the electron transfer among HRP molecules is not encountered.

The relative calculation of area coverage of HRPs on cerasome surface:

Assuming the head area of lipid in outer monolayer S_o^l and inner monolayer S_i^l are 0.74 and 0.61 nm^2, respectively [48]. The diameter of cerasome is 213 nm determined by DLS. Thus the radii of outer sphere and inner sphere in cerasome are 106.5 and 101.5 nm, respectively based on the thickness of lipid bilayer membrane, 5 nm.

The outer surface area of cerasome: $S_o = 4\pi r_o^2 = 4 \times 3.14 \times 106.5\ nm^2 = 1.42 \times 10^5$, $S_i = 4\pi r_i^2 = 4 \times 3.14 \times 101.5 nm^2$.

The number of lipids in one cerasome: $n = n_o + n_i = S_o^l/S_o + S_i^l/S_i = 1.42 \times 10^5 nm^2/0.74 nm^2 + 1.29 \times 10^5 nm^2/0.61 nm^2 = 4 \times 10^5$.

The mole of lipids in one cerasome: $N_{lipid} = n/N_A = 4 \times 10^5/(6.02 \times 10^{23}) = 6.64 \times 10^{-19} mol$.

The mole of HRP on electrode surface: $N_{HRP}^{electrode} = 5.7 \times 10^{-10}\ mol$.

The mole of HRP on each cerasome: $N_{HRP}^{cerasome} = 5.7 \times 10^{-10} mol/(3.7 \times 10^9) = 1.54 \times 10^{-19} mol$.

The diameter of HRP molecue is about 5 nm. So the sectional surface area of HRP: $S_s = \pi r_{HRP}^2 = 3.14 \times 2.5\ nm^2 = 19.6\ nm^2$.

The total sectional surface area of HRP: $S_T = S_s \times 1.54 \times 10^{-19} mol \times 6.02 \times 10^{23} = 1.82 \times 10^6 nm^2$.

The surface coverage of HRP on one cerasome is calculated to be $1.82 \times 10^6 nm^2/(1.42 \times 10^5 nm^2) \times 100\% = 1.28 \times 10^3\%$.

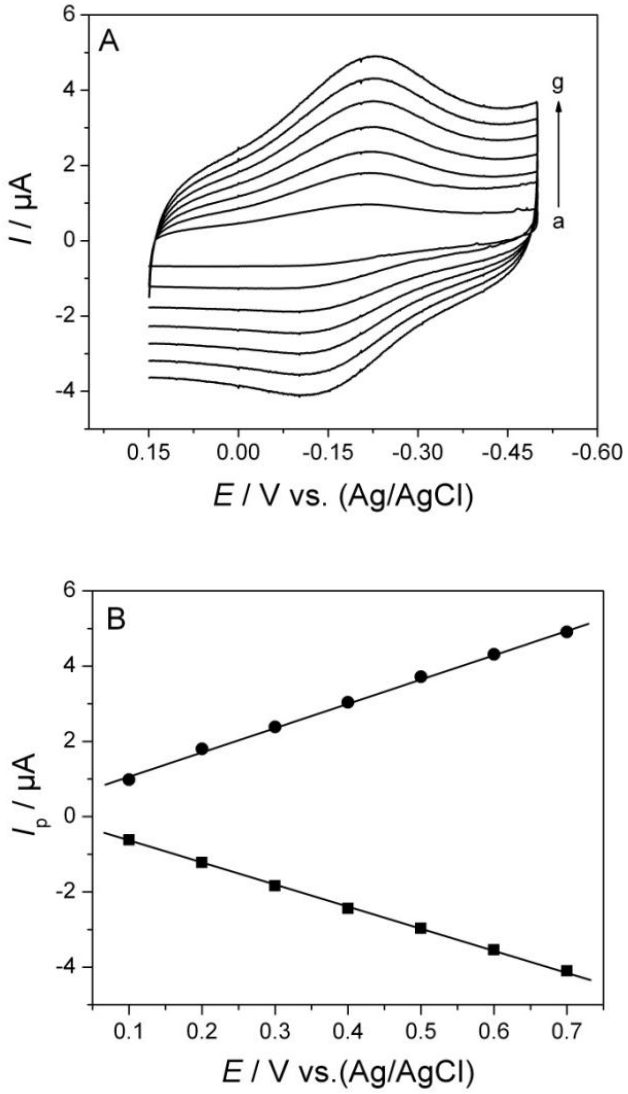

Figure 2-8. (A) CVs of HRP/cerasome/GCE electrode at the scan rates of 100, 200, 300, 400, 500, 600, 700 mV s^{-1} from a to g in 0.1 M citrate buffer solution (pH 5.6), respectively. **(B)** Plots of oxidation peak current (■) and reduction peak current (●) versus scan rate for HRP/cerasome/GCE electrode.

2. 3. 5 Electrocatalytic behaviors of electrode modified with cerasome and enzyme toward hydrogen peroxide

The investigation on the function of enzymatic biocatalysis has been served as the basis of the fabrication of a biosensor. Herein, I investigated the signal response of immobilized HRP toward hydrogen peroxide in detail. It is found that the cathodic peak

current at about -0.187 V is significantly enhanced with increasing the concentration of H_2O_2 as shown in **Figure 2-9 (A)**, indicating that the immobilized HRP exhibits its bioelectrocatalytic activity. Likewise, the cathodic peaks are shifted to negative potentials in the presence of H_2O_2 compared with the redox peak for HRP in absence of H_2O_2, which suggests some new chemicals are generated during the redox process. The possible electrocatalytic reaction between H_2O_2 and HRP is presented as follows [49]:

$$HRP(Fe^{3+}) + H_2O_2 \longrightarrow \text{Compound I } (Fe^{4+}=O) + H_2O \quad (1)$$

$$\text{Compound I } (Fe^{4+}=O) + e^- + H^+ \longrightarrow \text{Compound II} \quad (2)$$

$$\text{Compound II} + e^- + H^+ \longrightarrow HRP(Fe^{3+}) + H_2O_2 \quad (3)$$

The overall reaction would be

$$H_2O_2 + 2e^- + H^+ \longrightarrow 2H_2O \quad (4)$$

Firstly, hydrogen peroxidase reacts with the heme(Fe^{3+}) to release one water molecule and form the first intermediate (compound I) having an oxyferryl species (Fe^{4+}=O) and a porphyrin radical cation. And then the porphyrin radical cation undergoes reduction to form a second enzyme intermediate (compound II), which is subsequently converted back to the native HRP through a single electron transfer [50, 51].

Base on the chemical signal transduction, above described modified electrode could successfully achieve the detection of H_2O_2. There is a linear relation of the reduction peak currents with concentration of H_2O_2 in the range of 2.5~150 μM (correlation coefficient 0.9964, n = 15) in **Figure 2-9 (B)**. The detect limitation of HRP/cerasome/GCE is calculated at 0.83 μM based on the signal/noise ratio of (S/N = 3).

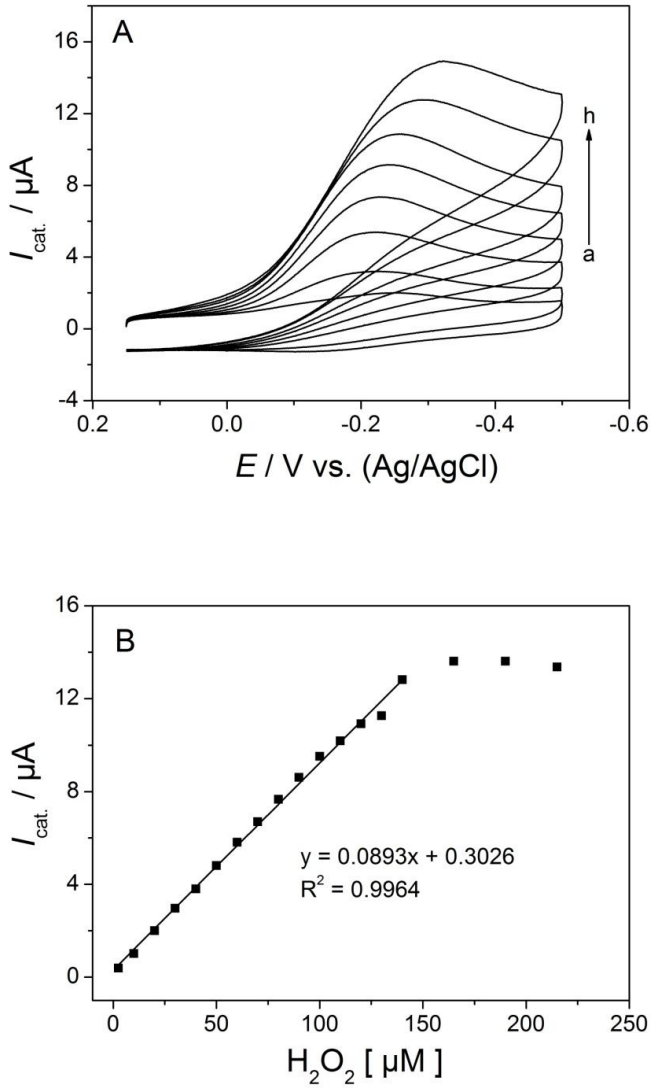

Figure 2-9. (A) CVs of HRP/cerasome/GCE modified electrode in pH 5.6 citrate buffer solution with the different concentrations of H_2O_2 from a to h: 0, 10, 30, 50, 70, 90, 110, and 135 μM. **(B)** Corresponding plots of the electrocatalytic current vs. H_2O_2 concentration.

3. 3. 6 Electrocatalytic response of electrode mobilized with cerasome and enzyme toward sodium nitrite

Figure 2-10 shows the CVs of HRP/cerasome/GCE with and without nitrite in citrate buffer solution (pH 5.6). A pair of well redox peaks assigned to the redox couples of heme-Fe(III/II) are observed at approximately -0.17V. A new reduction peak appears at

-0.76V upon addition of $NaNO_2$ into electrolyte. It has been demonstrated the new peak caused by the reduction of NO produced by the disproportionation reaction of NO_2^- in acidic solution [52]. In the acidic medium with low pH value below 6.0, NO can be generated thermodynamically.

$$3NO_2^- + H_2O \rightleftharpoons 2NO + NO_3^- + 2OH^-$$

The mechanisms of the electrocatalytic reduction of NO at HRP/cerasome/GCE are suggested to be the follows: [53]

$$\text{HRP-Fe (III)} + e \longrightarrow \text{HRP-Fe (II)} \quad (1)$$

$$\text{HRP-Fe (II)} + NO \longrightarrow \text{HRP-Fe (II) - NO} \quad (2)$$

$$2\ \text{HRP-Fe (II) - NO} + 2\ e + 2\ H^+ \longrightarrow 2\ \text{HRP-Fe (II)} + H_2O + N_2O \quad (3)$$

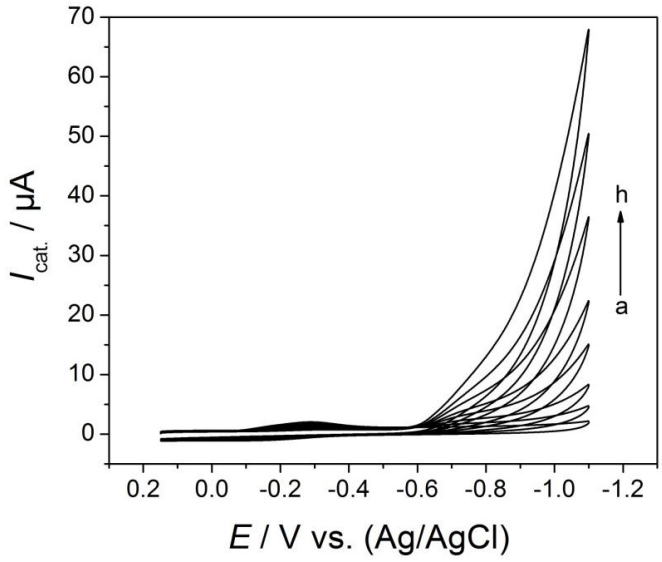

Figure 2-10. CVs of HRP/cerasome/GCE modified electrode in 0.1 M pH 5.6 citrate buffer solution containing $NaNO_2$: (a) 0, (b) 2.6, (c) 5.6, (d) 11.6, (e) 17.6, (f) 32.6, (g) 35.6, (h) 67.6 mM.

The amperometric responses of the HRP/cerasome/GCE toward sodium nitrite were also investigated by successively adding $NaNO_2$ to a continuous stirring citrate solution

at an applied potential of -0.8 V shown in **Figure 2-11 (A)**. Upon addition of an aliquot of $NaNO_2$ to the buffer, the reduction current of NO_2^- increases steeply and then reaches a stable value less than 4s, suggesting HPR/cerasome modified electrode has a fast response toward NO_2^-. **Figure 2-11 (B)** shows the calibration curve of the HRP/cerasome/GCE modified electrode. The linear response range of the sensor to $NaNO_2$ concentration is from 2.5 to 325 mM with a correlation coefficient of 0.9981 (n = 24) with the detection limit of 0.83 mM estimated at signal-to-noise of 3.

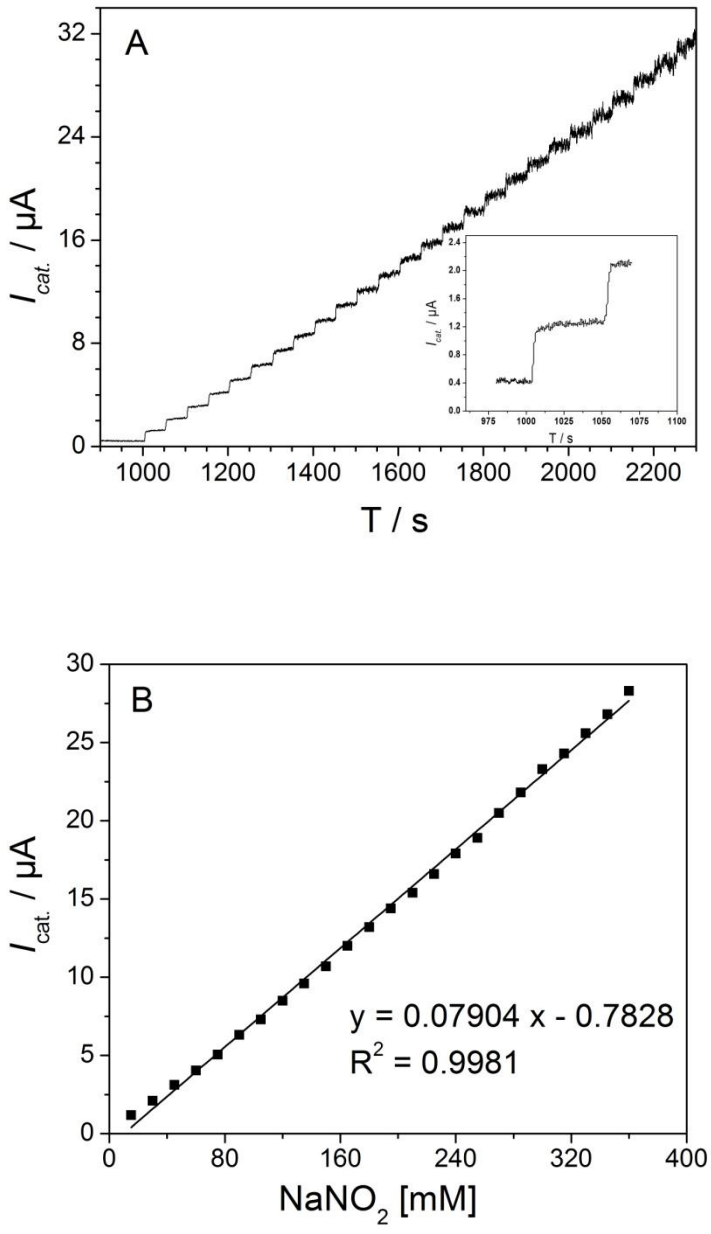

Figure 2-11. (A) current-time curves for successive addition of 15 mM $NaNO_2$ in citrate buffer solution at applied potential of -0.8 V (vs. Ag/AgCl) and (**B**) calibration plots of the HRP/cerasome/GCE electrode as a function of $NaNO_2$ concentrations.

2. 4 Conclusions

Cerasome was a novel organic-inorganic nanohybrid material, which exhibited high morphological stability. The results of SEM and TEM indicated that cerasome can keep spherical structure as silica NP. In addition, cerasome had the lipid bilayer membrane structure, which enhanced its biocompatibility. The siloxane networks on the surface of cerasome gave rise to well water solubility. Because of these fine characters, as a matrix, HRP could be effectively immobilized on cerasome without diminishing its bioactivity. Thus, cerasome could provide an efficient platform for electron transfer and the HRP/cerasome/GCE electrochemical interface exhibited good electrochemical property. Moreover, the immobilized HRP on cerasome/GCE was found to retain the catalytic activity for H_2O_2. However, because of structural defect of liposome and silica NP, electron transfer on both HRP/silica NP/GCE and HRP/liposome/GCE modified electrode were hard to achieve. Thus, comparing to the traditional liposome and silica NP, cerasome can support a more stable and biocompatible environment to protect the deactivation of HRP molecular, which make it possible to become a potential biomaterials.

2. 5 References

[1] Nicholls D G, Ferguson S J, Ferguson S. Bioenergetics. 3th ed. Academic Press, New York, 2002.

[2] Frew J E, Hill H A O. Direct and indirect electron transfer between electrodes and redox proteins. Eur. J. Biochem. 1988; 172: 261-269.

[3] Lötzbeyer T, Schuhmann W, Schmidt H L. Electron transfer principles in amperometric biosensors: direct electron transfer between enzymes and electrode surface. Sensor Actuat. B-Chem. 1996; 33: 50-54.

[4] Anderson J L, Bowden E F, Pickup P G. Dynamic electrochemistry: methodology and application. Anal. Chem. 1996; 68: 379R-444R.

[5] Armstrong F A, Heering H A, Hirst J. Reactions of complex metalloproteins studied by protein-film voltammetry. Chem. Soc. Rev. 1997; 26: 169-179.

[6] Fraser A, Armstrong H, Hill A O, Walton N G. Direct electrochemistry of redox proteins. Acc. Chem. Res. 1988; 21: 407-413.

[7] Rusling J F, Nassar A E F. Enhanced electron transfer for myoylobin in surfactant films on electrodes. J. Am. Chem. Soc. 1993; 115: 11891-11897.

[8] Ottova A, Thien H T, Ottova-Leitmannova A. In advance in planar lipid bilayer and liposome. Academic press, 2005; 1: 1-76.

[9] Alberts B, Johnson A, Lewis J, Raff M. Molecular biology of the cell. 5th ed. Chapter 15th, Garland Science: Taylor & Francis Group, 2008.

[10] Dimitrios P N, Tibor H, Ulrich J K. Biosensor based on thin lipid films and liposome. Electroanalysis 1999; 11: 7-15.

[11] Bally B, Bailey K, Sugihara K, Grieshaber D, Vörös J, Städler B. Liposome and lipid bilayer arrays towards biosensing applications. Small 2010; 6: 2481-2497.

[12] Munishwar N G, Mandeep K, Manali K, Kusum S. Nanomaterials as matrices for enzyme immobilization. Artif. Cell Blood Substit. Biotechnol. 2011; 39: 98-109.

[13] Shakeel A A, Qayyum H. Potential applications of enzymes immobilized on/in nano materials: a review biotechnology advances. Biotechno. Adv. 2012; 30: 512-523.

[14] Lei J P, Ju H X. Signal amplification using functional nanomaterial for biosensing. Chem. Soc. Rev. 2012; 41: 2122-2134.

[15] Katagiri K, Ariga K, Kikuchi J. Preparation of organic-inorganic hybrid vesicle "cerasome" derived from artificial lipid with alkoxysilyl head. Chem. Lett. 1999; 28: 661-662.

[16] Hashizume M, Kawanami S, Iwamoto S, Isomoto I, Kikuchi J. Stable vesicular nanoparticle 'Cerasome' as an organic-inorganic hybrid formed with organoalkoxysilane lipids having a hydrogen-bonding unit. Thin Solid Film 2003; 438-439: 20-26.

[17] Matsui K, Sando S, Sera T, Aoyama Y, Sasaki Y, Komatsu T, Terashima T, Kikuchi J. Cerasome as an infusible cell-friendly and serum-compatible transfection agent in a viral size. J. Am. Chem. Soc. 2006; 128: 3114-3115.

[18] Sasaki Y, Matsui K, Aoyama Y, Kikuchi J. Cerasome as an infusible and cell-friendly gene carrier: Synthesis of cerasome-forming lipids and transfection using cerasome. Nat. Protocols 2006; 1: 1227-1234.

[19] Kikuchi J, Yasuhara K, in Advances in Biomimetics, ed. by A. George, In Tech, Rijeka, 2011, pp 231-250.

[20] Katagiri K, Hamasaki R, Ariga K, Kikuchi J. Preparation and surface modification of novel vesicular nano-particle "cerasome" with liposomal bilayer and silicate

surface. J. Sol-Gel Sci. Technol. 2003; 26: 393-396.

[21] Tahara K, Moriuchi T, Tsukui M, Hirota A, Maeno T. Ceramic coating of liposomal gene carrier for minimizing toxicity to primary hippocampal neurons. Chem. Lett. 2013; 42: 1265-1267.

[22] Tian W J, Sasaki Y, Sheng D I, Fan S D, Kikuchi J. Switching of enzymatic activity through functional connection of molecular recognition on lipid bilayer membrane. Supramol. Chem. 2005; 17: 113-119,

[23] Sasaki Y, Yamada M, Terashima T, Wang J F, Hashizume M, Fan S D, Kikuchi J. Construction of intermolecular communication system on "cerasome" as an organic-inorganic nanohybrid. Kobunshi Ronbunshu 2004; 61: 541-546.

[24] Nishimori H, Tatsumisago M, Minami T. Growth mechanism of large monodispersed silica particles prepared from tetraethoxysilane in the presence of sodium dodecyl sulfate. J. Sol-Gel Sci. Technol. 1997; 9: 25-31.

[25] Welinder K G. Amino acid sequence studies of horseradish peroxidase. Eur. J. Biochem. 1979: 96: 483-502.

[26] Talmon Y. Transmission electron microscopy of complex fluids: the state of the art. Ber. Bunsenges. Phys. Chem. 1996; 100: 364-372.

[27] Almgren M, Edwards K, Gustafsson J. Cryotransmission electron microscopy of thin vitrified samples. Curr. Opin. Colloid Interface Sci. 1996; 1: 270-278.

[28] Almgren M, Edwards K, Karlsson G. Cyrotransmission electron microscopy of liposome and related structures. Colloids and Surfaces 2000; 174: 3-21.

[29] Mornet S, Lambert O, Duguet E, Brisson A. The formation of supported Lipid bilayers on silica nanoparticles revealed by cryoelectron microscopy. Nano. Lett. 2005; 5:281-285.

[30] Butler S, Wang R W, Wunder S L, Cheng H Y, Randall C S. Perturbing effects of carvedilol on a model membrane system: role of lipophilicity and chemical structure. Biophys. Chem. 2006; 119: 307-315.

[31] Smith G S, Sirota E B, Safinya C R, Plano R J, Clark N A. X-ray structural studies of freely suspended ordered hydrated DMPC multimembrane films. J. Chem. Phys. 1990; 92: 4519-4529.

[32] Zhang Q, Qiao Y, Hao F, Zhang L, Wu S Y, Li Y, Li J H, Song X M. Fabrication of a biocompatible and conductive platform based on single-stranded DNA/Graphene nanocomposite for direct electrochemistry and electrocatalysis. Chem. Eur. J. 2010; 16: 8133-8139.

[33] Sears D W, Beychoch S. In physical principles and techniques of protein chemistry, ed. by Leach S J, New York London: academic press, 1973, pp 445-593.

[34] Myer Y P. Conformation of cytochromes. II. Comparative study of circular dichroism spectra, optical rotatory dispersion, and absorption spectra of horse heart cytochrome c. J. Biol. Chem. 1968; 243: 2115-2122.

[35] Chattopadhyay K, Mazumdar S. Structural and conformational stability of horseradish peroxidase: effect of temperature and pH. Biochemistry 2000; 39: 263-270.

[36] Hsu M C, Woody R W. Origin of the heme Cotton effects in myoglobin and hemoglobin. J. Am. Chem. Soc. 1971; 93: 3515-3525.

[37] Rusling J F. Enzyme bioelectrochemsitry in cast biomembrane-like films. Acc. Chem. Res. 1998; 31: 363-369.

[38] Kang X H, Wang J, Tang Z W, Wu H, Lin Y H. Direct electrochemistry and electrocatalysis of horseradish peroxidase immobilized in hybrid organic-inorganic

film of chitosan/sol-gel/carbon nanotubes. Talanta 2009; 78: 120-125.

[39] Marcus R A. Electron transfer reactions in chemistry: theory and experiment (Nobel Lecture). Angew. Chem. Int. Ed. Engl. 1993; 32: 1111-1121.

[40] Marcus R A, Sutin N. Electron transfers in chemistry and biology. Biochimica. et Biopgysica. Acta. 1985; 811: 265-322.

[41] Levich V G. Present state of the theory of oxidation-reduction reactions in solution (bulk and electrode reactions). Adv. Electrochem. Sci. Eng. 1966; 4: 249.

[42] Heller A. Electrical wiring of redox enzymes. Acc. Chem. Res. 1990; 23: 128-134.

[43] Vertegel A A, Siegel R W, Dordick J S. Silica nanoparticles size influences the structure and enzymatic activity of adsorbed lysozyme. Langmuir 2004; 20: 6800-6807.

[44] Ling X L, Xue X L, Dai Z F, Kikuchi J. photoreponsive liposomal nanohybrid cerasome. Chem. Commun. 2011; 47: 4751-4753.

[45] Ma Y, Dai Z F, Gao Y G, Cao Z, Zha Z B, Xue X L, Kikuchi J. Liposomal architecture boosts biocompatibility of nanohybrid cerasomes. Nanotoxicology. 2011; 5: 622-635.

[46] Wang S F, Chen T, Zhang Z L, Shen X C, Lu Z X, Pang D W, Wong K Y. Direct Electrochemistry and electrocatalysis of heme proteins entrapped in agarose hydrogel films in room-temperature ionic liquids. Langmuir 2005; 21: 9260-9266.

[47] Zhang L, Zhang Q, Lu X B, Li J H. Direct electrochemistry and electrocatalysis based on film of horseradish peroxidase intercalated into layered titanate nano-sheets. Biosens. Bioelectron. 2007; 23: 102-106.

[48] Huang C, Mason J T. Geometric packing constraints in egg phosphatidylcholine vesicles. Proc. Natl. Acad. Sci. USA 1978; 75: 308-310.

[49] Zeng X D, Wei W Z, Li X F, Zeng J X, Wu L. Direct electrochemistry and electrocatalysis of hemoglobin entrapped in semi-interpenetrating polymer network hydrogel based on polyacrylamide and chitosan. Bioelectrochemistry 2007; 71: 135-141.

[50] Rodriguez-Lopez J N, Lowe D J, Hernandez-Ruiz J H, Hiner A N P, Carcia-Canovas F, Thorneley R N F. Mechanism of reaction of hydrogen peroxide with horseradish peroxidase: identification of intermediates in the catalytic cycle. J. Am. Chem. Soc. 2001; 123: 11838-11847.

[51] Dunford H B, Stillman J S. On the function and mechanism of action of peroxidases. 1976; 19: 187-251.

[52] Bayachou M, Lin R, Cho W, Farmer P J. Electrochemical reduction of NO by myoglobin in surfactant film: characterization and reactivity of the nitroxyl (NO^-) adduct. J. Am. Chem. Soc. 1998; 120: 9888-9893.

[53] Xu Y X, Hu C G, Hu S S. Direct electron-transfer of native hemoglobin in blood: Kinetics and catalysis. Bioelectrochemsitry 2008; 72: 135-140.

Chapter 3. Design and characterization of electroactive cerasome modified with artificial coenzyme

3. 1 Introduction

Vitamin B_{12} derivative is a unique coenzyme, involving the cobalt species as catalytic center. It is recently attracted attention in the field of electrocatalysis, because it effectively mediates various isomerization reactions accompanied by carbon-skeleton intramolecular rearrangements including an exchange of a functional group (X) and a hydrogen atom on adjacent carbon atoms in equation (1) [1-3].

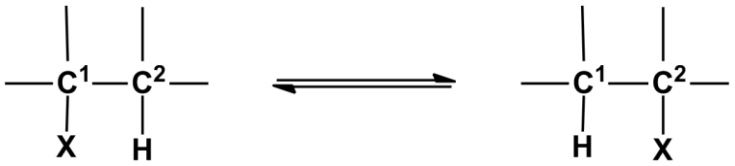

(1)

In order to simulate these relevant reactions and investigate the function of vitamin B_{12} as exerted in the hydrophobic reaction active sites of enzymes concerned, Murakami, et al. prepared hydrophobic vitamin B_{12} (HVB_{12}) derivatives which have ester group instead of the peripheral amide moieties of natural vitamin B_{12}. They can easily dissolve in series of organic solvent [4-9].

Up to now, several types of complexes of artificial B_{12} enzyme were prepared by combing the HVB_{12} with other materials such as bilayer membrane, silica gel and so on. Among them, the vesicle-type artificial holoenzyme was one outstanding example composed of peptide lipids and HVB_{12} [5, 8, 10]. In this artificial enzyme, bilayer membrane provided a favorable microenvironment for both HVB_{12} and substrate molecules, and ensured catalysis reaction perform smoothly. Up to now, numerous peptide lipids were designed and synthesized, such as peptide lipid, $N^+C_5Ala2C_{16}$. They formed a relatively stable vesicle because of amino acid residue interposed between a

polar head moiety and a hydrophobic double-chain segment, which enhanced the morphological stability [11-13]. A large number of research works on the electrocatalytic behaviors of HVB_{12} dependent vesicle-type artificial holoenzyme in solution have been carried out [8]. However, there were no reports on electrochemical behaviors of artificial holoenzyme deposited on electrode surface, because liposomal vesicles easily lost their structure.

On condition that catalyst is immobilized on the electrode surface it offers an efficient use of catalyst for electroorganic synthesis [14-16]. From this view point, study on the electrochemical properties of immobilized HVB_{12} incorporated into the vesicle on the electrode is significantly meaningful. However, the key point of achievement of this purpose is to seek a new stably liposomal nanomaterial instead of liposome and develop a stable vesicle-type HVB_{12} coenzyme. Fortunately, in our research laboratory a highly stable hybrid cerasome with ceramic surface was developed. It is bio-inspired colloidal particles having an inner aqueous compartment like the liposomal membrane. Besides, its surface is covered by the inorganic siloxane framework, which imparts it higher stable morphology than traditional liposome [17-20]. Because of this specific physical property we have exploited metallic cerasome coated with thin metal film such as titania, silver, FeCoNi alloy [18, 21-22]. Photoresponsive cerasome has also been brought out through covalent or non-covalent modification [23-25]. However, the potential of cerasome for electroactivity has been not developed by now. Due to these reasons I integrated cerasome with HVB_{12}. On one hand, this work can produce more stably artificial hydrophobic vitamin B_{12} dependent enzyme, on the other hand, it offers an opportunity to open up a new ceracome with novel function.

In this chapter, I firstly designed a novel electroactive nanohybrid cerasome through incorporating HVB_{12} into the lipid bilayer membrane of cerasome, and then investigated its electrochemical functions. The formation of electroactive nanohybrid cerasome incorporated HVB_{12} was confirmed by UV-vis spectroscopy and differential scanning calorimetry (DSC). The morphologies of hybrid cerasome were directly observed by atomic force microscopy (AFM) on the solid surface. To examine the electroactive property of the resulting electroactive nanohybrid cerasome, I fabricated an electrochemical interface on glassy carbon electrode using HVB_{12}-cerasome (**Scheme 3-1**). Additionally, the cyclic voltammetry was used to evaluate the electrocatalytic functions of this electrochemical interface toward substrates, such as iodomethane, in aqueous solution.

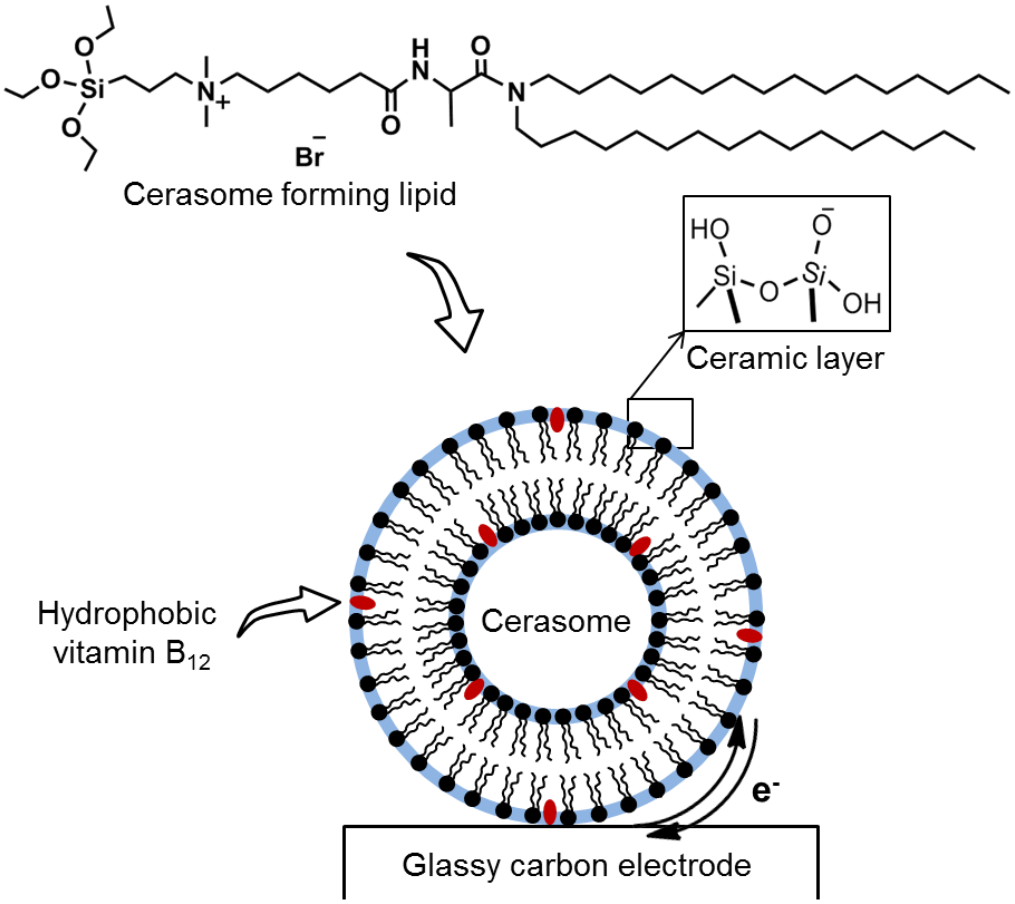

Scheme 3-1. Chemical structure of cerasome forming lipid and schematic illustration of HVB_{12}-cerasome/GCE electrochemical interface.

3. 2 Experiments

3. 2. 1 Materials

Hydrophobic vitamin B_{12} derivatives, [Cob(II)7C_3ester]ClO_4 was synthesized from cyanocobalamin with reference to the methods reported [5] by Biofunctional Chemistry Group, Department of Chemistry and Biochemistry Graduate School of Engineering, Kyushu University and used as-received state without any purification further. Cationic cerasome-forming lipid, *N*, *N*-dihexadecyl-N^{α}-(6-((3-triethoxysilyl) propyldimethylam-momio)hexanoyl)alanineamide bromide was synthesized according to previous reported in our laboratory [20]. *N*-(t-butoxycarbonyl)alanine was purchased from Peptide Institute. 6-bromohexanoyl chloride, trifluoroacetic acid (**TFA**), and dimethylamine were obtained from Sigma-Aldrich. 3-bromopropyltriethoxysilane was obtained from Shin-Estu Chemical Co., Ltd. Potassium poly(vinyl sulfate) (**PVS**), and poly(diallyldimethylammonium chloride) (**PDDA**) were purchased from Wako Pure Chemical Industries. The phosphate buffer solution (PBS 0.1 M, pH = 7) was prepared from Na_2HPO_4 and NaH_2PO_4. The water used in all experiments was deionized using a Milli-Q Labo (Nihon Milipore).

3. 2. 2 Synthesis of cationic cerasome-forming lipid

N, *N*-dihexadecyl-N^{α}-6-((3-triethoxysilyl)propyldimethylammomio)hexanoyl)alanine amide bromide was synthesized in five-step method according to previous report in our laboratory shown in **scheme 3-1**. The detailed synthesis procedures of cationic cerasome-forming lipid were performed as follows:

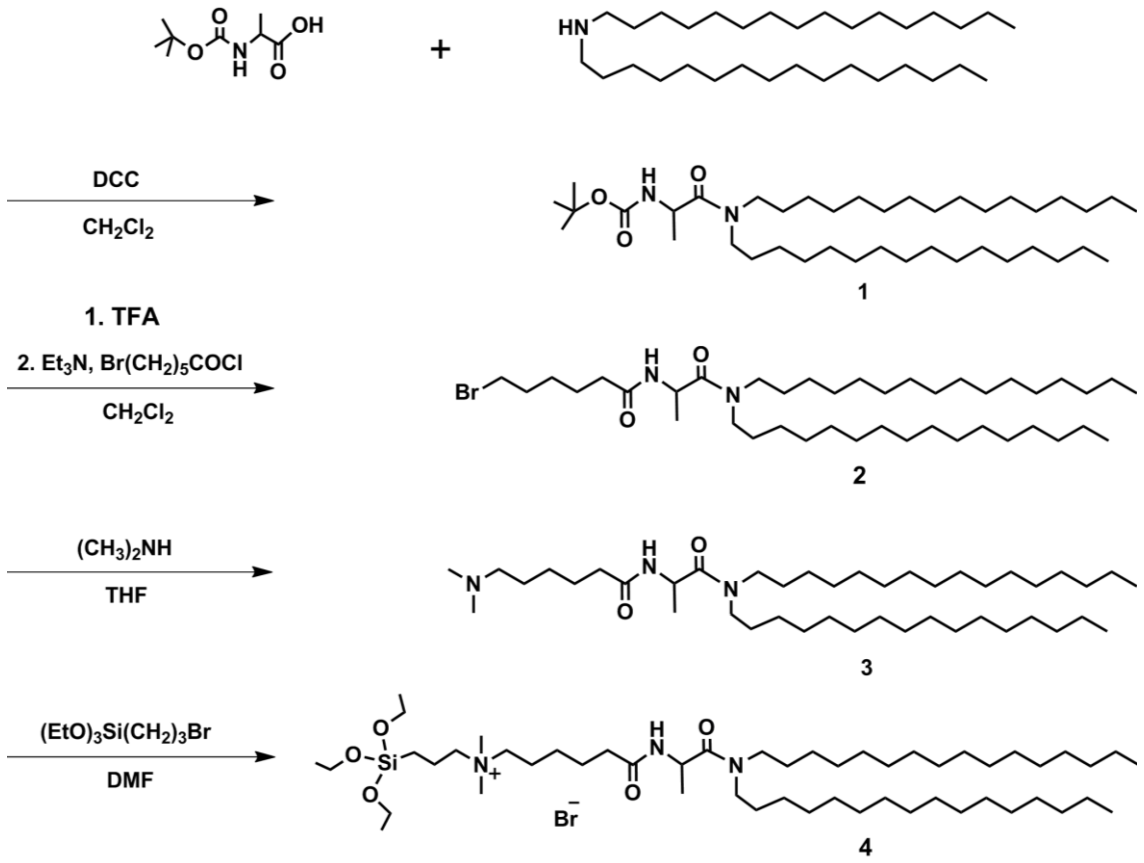

Scheme 3-2. Synthesis of cationic cerasome-forming lipid.

N, *N*-dihexadecyl-N^{α}-(t-butoxycarbonyl)alaninamide (Product 1)

To a solution of *N*-(t-butoxycarbonal)alanine (2.19 g, 11.6 mmol) in 80 ml of dry CH_2Cl_2, DCC (2.41 g, 11.7 mmol) was added. After stirring for 15 min at 0 °C, *N*,*N*-dihexadecylamine was added into above solution. This mixture was stirred at 0 °C for 4 h and then 15 h further at room temperature. The precipitate, *N*, *N*-dicyclohexylurea, was then removed by filtration with filter paper. The solvent was evaporated off with rotary evaporator vacuum. After that the residual colorless oil was dissolved in ethyl acetate followed work up with saturated NaCl solution, citric acid (10%), $NaHCO_3$ (4%) in turn. Finally this crude product was purified by silica chromatography column with hexane-ethyl acetate (9:1 v/v). The yield is 3.51g (55.7%).

TLC: R_f = 0.52 [silica gel 60F254 plate Merck, hexane: ethyl acetate (6:1, v/v)] ^{1}H-NMR (400 MHz, $CDCl_3$, TMS): δ 0.88 [6H, t, *J* = 6.8 Hz, $NCH_2CH_2(CH_2)_{13}CH_3$], 1.25-1.30 [52H, m, $NCH_2CH_2(CH_2)_{13}CH_3$], 1.29 [3H, d, *J* = 6.8 Hz, $NHCHCH_3$], 1.43 [9H, s, $(CH_3)_3$ CO], 1.57 [4H, m, $NCH_2CH_2(CH_2)_{13}CH_3$], 3.13 [1H, m, $NCHHCH_2(CH_2)_{13}CH_3$], 3.24 [2H, t, *J* = 7.2 Hz, $NCH_2CH_2(CH_2)_{13}CH_3$], 3.44 [1H, m, $NCHHCH_2(CH_2)_{13}CH_3$], 4.57 [1H, m, *J* = 7.2Hz $NHCHCH_3$], 5.45 [1H, d, *J* = 7.8 Hz, $NHCHCH_3$].

***N*, *N*-Dihexadecyl-N^{α}-(6-bromohexanoyl)alaninamide (Product 2)**

TFA (5.4 g, 47.1 mmol) was added into 30 ml of dry CH_2Cl_2 with product **1** (3.32 g, 5.17 mmol). The above mixture was stirred for 5 h at room temperature. The excess TFA and CH_2Cl_2 were removed under reduced pressure to give pale yellow oil. The residual oil and triethylamine (1.84 g, 18.1 mmol) was dissolved in 20 ml of dry CH_2Cl_2 at 0 °C. Then 20 ml of dry CH_2Cl_2 solution in presence of 6-bromohexanoyl chloride (3.5 g, 16.88 mmol) was added dropwise. The mixture was stirred for 4 h at 0 °C and 8 h further at room temperature. The solution was washed sequentially with saturated sodium chloride solution, citric acid solution (5%), sodium hydrogen carbonate solution (4%), and saturated sodium chloride solution. The yield is 0.94g (23.5%).TLC: R_f = 0. 36 [silica gel 60F254 plate Merck, hexane: ethyl acetate (5/2, v/v)] ^{1}H-NMR (400 MHz, $CDCl_3$, TMS): δ 0.88 [6H, t, *J* = 6.8 Hz, $NCH_2CH_2(CH_2)_{13}CH_3$], 1.25-1.31 [52H, m, $NCH_2CH_2(CH_2)_{13}CH_3$], 1.29 [3H, d, *J* = 8.1 $NHCHCH_3$], 1.41-1.52 [6H, m, $NCH_2CH_2(CH_2)_{13}CH_3$, $BrCH_2CH_2CH_2CH_2CH_2CO$], 1.68 [2H, m, $BrCH_2CH_2CH_2CH_2CH_2CO$], 1.88 [2H, quin, *J* = 7.6 Hz, $BrCH_2CH_2CH_2CH_2CH_2CO$], 2.2 [2H, t, $BrCH_2CH_2CH_2CH_2CH_2CO$], 3.12 [1H, m, $NCHHCH_2(CH_2)_{13}$ CH_3], 3.22 [2H, m, *J* = 7.8 $NCH_2CH_2(CH_2)_{13}CH_3$], 3.40 [2H, t, *J* = 6.7 Hz, $BrCH_2CH_2CH_2CH_2$

CH_2CO], 3.49 [1H, m, J_1 = 13.7, J = 7.3 Hz NC*H*H$CH_2(CH_2)_{13}CH_3$] 4.83 [1H, m, J = 7.1 Hz NHC*H*CH_3], 6.52 [1H, d, J = 7.8 Hz, N*H*$CHCH_3$].

***N*, *N*-Dihexadecyl-N^{α}-(6-(dimethylamino)hexanoyl)alaninamide (Product 3)**

Dry dimethylamine gas was introduced into product **2** (0.94 g, 1.32 mmol) solutions in dry THF (82 ml) until saturation. The mixture was stirred at room temperature for 72 h. Then removal of excess dimethylamine was performed by bubbling of N_2. The solvent was evaporated off *in vacuo*, and then the residual solid was dissolved in chloroform (50 ml). After that the solution was washed with saturated sodium chloride solution, sodium hydrogen carbonate solution (4%) and saturated sodium chloride solution sequentially. The solvent was evaporated off in vacuum drier after removal of water by phase separation filter paper. Finally the residue purified by recrystallization from acetonitrile.

Yield is 0.101g (13.5%) TLC: R_f = 0.50 [silica gel 60F254 plate Merck, chloroform: methanol (4:1, v/v)] ^{1}H-NMR (400 MHz, $CDCl_3$, TMS): δ 0.88 [6H, t, J = 6.8 Hz, $NCH_2CH_2(CH_2)_{13}CH_3$], 1.25-1.51 [54H, m, NCH_2CH_2 $(CH_2)_{13}CH_3$, $(CH_3)_2NCH_2CH_2CH_2CH_2CH_2CO$], 1.31 [3H, d, J = 6.9 Hz, $NHCHCH_3$], 1.45-1.54 [6H, m, $NCH_2CH_2(CH_2)_{13}CH_3$, $(CH_3)_2NCH_2CH_2CH_2CH_2CH_2CO$], 1.61-1.69 [2H, m, $(CH_3)_2NCH_2CH_2CH_2CH_2CH_2CO$], 2.19 [2H, t, J = 7.7 Hz, $(CH_3)_2NCH_2CH_2$ $CH_2CH_2CH_2CO$], 2.20 [6H, s, $(CH_3)_2NCH_2CH_2CH_2CH_2CH_2CO$], 2.24 [2H, t, $(CH_3)_2NCH_2CH_2CH_2CH_2CH_2CO$], 3.09 [1H, m, NC*H*H$CH_2(CH_2)_{13}CH_3$], 3.21 [1H, m, NC*H*H$CH_2(CH_2)_{13}CH_3$], 3.24 [1H, m, NC*H*H$CH_2(CH_2)_{13}CH_3$], 3.49 [1H, m, NC*H*H $CH_2(CH_2)_{13}CH_3$], 4.84 [1H, m, NHC*H*CH_3], 6.51 [1H, d, J = 7.1 Hz, N*H* $CHCH_3$].

***N*, *N*-Dihexadecyl-N^{α}-(6-((3-triethoxysilyl)propyldimethylammonio)hexanoyl)Alaninamide bromide (Product 4)**

To a solution of product **3** (0.1 g, 0.15 mmol) in dry DMF (30 mL), 3-bromopropyltriethoxy silane (0.22 g, 0.78 mmol) was added and the mixture was stirred at room temperature for 72 h under a nitrogen atmosphere. The solvent was evaporated off *in vacuo* and the residue was purified on a column of silica gel (Wako gel C-300) with an eluent of chloroform-methanol (3:1, v/v). The colorless oil was obtained. The yield is 58 mg (40%); R_f = 0.47 [silica gel 60F254 plate Merck, chloroform–methanol (3:1 v/v)]; ^{1}H-NMR (400 MHz, $CDCl_3$, TMS): δ 0.66 [2H, t, *J* = 7.6 Hz, $SiCH_2$], 0.87 [6H, t, *J* = 6.8 Hz, $NCH_2CH_2(CH_2)_{13}CH_3$], 1.22 [9H, t, *J* = 6.8 Hz, $(CH_3CH_2)_3Si$], 1.21-1.34 [54H, m, $NCH_2CH_2(CH_2)_{13}CH_3$, $N^+CH_2CH_2CH_2CH_2CH_2CO$], 1.32 [3H, d, *J* = 6.3 Hz, NHCH CH_3], 1.40-1.52 [4H, m, $NCH_2CH_2(CH_2)_{13}CH_3$], 1.67-1.83 [6H, m, $SiCH_2CH_2CH_2N^+$ $CH_2CH_2CH_2CH_2CH_2CO$], 2.27 [1H, m, $N^+CH_2CH_2CH_2CH_2CHHCO$], 2.34 [1H, m, J_1= 15.1 Hz, J_2 = 7.3 Hz N^+ $CH_2CH_2CH_2CH_2CHHCO$], 3.08 [1H, m, $NCHHCH_2(CH_2)_{13}CH_3$], 3.24 [2H, m, NCH_2 $CH_2(CH_2)_{13}CH_3$], 3.35 [6H, d, $(CH_3)_2N^+CH_2CH_2CH_2CH_2CH_2CO$], 3.45-3.53 [5H, m, $NCHHCH_2(CH_2)_{13}CH_3$, $SiCH_2CH_2CH_2N^+CH_2CH_2CH_2CH_2CH_2CO$], 3.82 [6H, quar, *J* = 7.0 Hz, $(CH_3CH_2)_3Si$], 4.76 [1H, quin, *J* = 7.0 Hz, $NHCHCH_3$], 6.9 [1H, d, *J* = 6.6 Hz, $NHCHCH_3$].

3. 2. 3 Measurements

^{1}H-NMR spectra were recorded on a JEOL JNM-EPC400NK spectrometer. Absorbance measurements were performed on **UV-vis** spectrophotometer (Jasco, V-670). The morphologies of samples were observed by atomic force microscopy (**AFM**, SPI-3800N, Seiko Instruments Inc., Japan) in the tapping mode with a 20 μm

scanner in ambient atmosphere. The samples for AFM observations were prepared by layer-by-layer method on fresh cleaved mica surface [26]. Fresh cleaved mica was immobilized by cationic (PDDA) and anionic (PVS) polymer alternately, starting from PDDA and terminating by PVS.

Differential scanning calorimetry (**DSC**) was conducted using a VP-DSC micro-calorimeter (MiroCal LLC) with the scanning rate of 0.5 °C/min in the range of 5 ~ 45 °C. The phase transition temperature (T_m) and enthalpy change for the transition (ΔH) were determined from the thermograms.

Cyclic voltammetry (**CV**) measurements were performed on CHI 630d electrochemical analyzer with a three-electrode cell, composed of a Pt wire counter electrode, an Ag/AgCl reference electrode, cerasome/GCE and HVB_{12}-cerasome/GCE modified electrode as working electrode at room temperature. A phosphate buffer solution with pH 7 (with 0.1 M KCl) was used as electrolyte. The electrolyte was deaerated using highly pure nitrogen for at least 30 min to remove the dissolved oxygen. The nitrogen atmosphere was kept during all the electrochemical experiments.

3. 2. 4 Preparation of nanohybrid formed by cerasome and hydrophobic vitamin B_{12}

HVB_{12} functionalized cerasome was prepared according to the Bangham method [27] by self-assembly of organoalkoxysilylated lipids and HVB_{12} derivatives, [Co(II)7C_3ester]ClO_4, which has propyl ester groups on place of the peripheral amid moieties of the naturally occurring vitamin B_{12}. Firstly, hydration of the mixture film of 100 μL of lipid **1** (10 mM, in chloroform) and 3 μL of vitamin B_{12} (5 mM, in ethanol) with Milli-Q water (40 °C) gave a slightly turbid HVB_{12}-cerasome dispersion. And then the resulting dispersion was subjected to probe sonication for 2 min at the power of 40 W to get a clear lightly pink solution. To precipitate metal particles from sonication

probe the aqueous dispersion were centrifuged at the speed of 5000 rpm for 10 min. All of samples were incubated for 24 h at room temperature to confirm the good condensation of ethoxysilyl group before use. The final molar ratio of lipid and HVB_{12} was controlled at 100: 1.5. Cerasome was prepared with the same procedure as describe above. The sample used for the DSC measurement was not processed by sonication but treated with freeze-and-thaw (-193 °C and 45 °C) for 10 cycles.

3. 2. 5 Fabrication of electrode modified with cerasome and hydrophobic vitamin B_{12}

Prior to use, glassy carbon electrode (GCE) with the diameter of 3 mm was polished on polishing cloth with 0.03 μm alumina powder and rinsed with deionized water followed 2 mins water bath sonication. The pretreated GCE was then dried at room temperature after casting 7 μL of HVB_{12}-cerasome dispersion, and covered with a beaker in order to evaporate water gradually. A thin film of HVB_{12}-cerasome was formed on the surface of electrode after the evaporation of water. The cerasome/GCE was prepared as the same procedure as described above.

3. 3 Results and discussion

3. 3. 1 Spectroscopic characterization of cerasome-artificial coenzyme nanohybrid

When the n-value of C_n in the ester groups situated at the peripheral sites of the corrinoid skeleton is more than or equal to 2, HVB_{12} derivative is nearly water insoluble [5]. The HVB_{12}, [Cob(II)7C_3ester]ClO_4, used in my work is almost insoluble in water due to n = 3. **Figure 3-1** shows the photographs of free (a) and incorporated (b) HVB_{12}, respectively in water solution. As can be seen, free HVB_{12} is aggreageted in water. While HVB_{12} moelecues are incorported into cerasome they disperse well in water to form a homogenously pink dispersion. This indicates that HVB_{12} molecules are completely embedded into lipid bilayer membrane of cerasome during the procedure of vesicle formation.

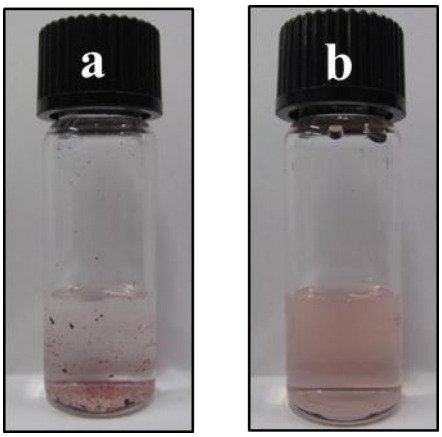

Figure 3-1. Photographs of free (a) and incorporated (b) HVB_{12} in water.

In order to prove that the HVB_{12} were embedded into cerasome membrane, the UV-vis spectroscopy was adopted here. **Figure 3-2** shows the UV-vis spectrum of HVB_{12}-cerasome dispersion in equeous solution. Since cobalt(II) in HVB_{12} are partially converted into cobalt(III) complex during the sonication a strong absorption brand is

observed clearly at 354 nm, which is attributable to the Co(III). These results are in consistant with the results of revious report [28]. The broaden peak at 466 nm is ascribed to the mixture of cobalt(II) and cobalt(III) complex. The UV-vis spectrum indicates that HVB_{12} molecules are successfully incorporated into the lipid bilayer of cerasome.

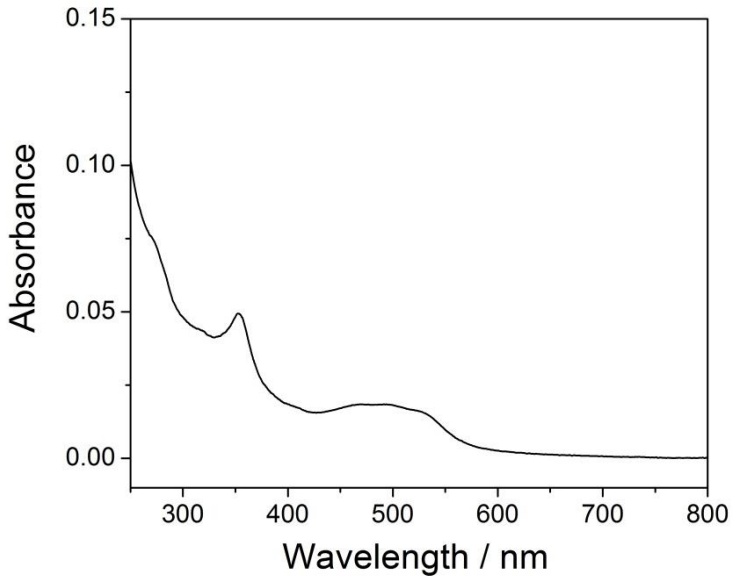

Figure 3-2. UV-vis sepectrum of HVB_{12}-cerasome in water.

3. 3. 2 Structural characterization of cerasome-artificial coenzyme nanohybrid.

AFM microscopy is a powerfull tool to observe the morphorlogy of materials under nomarl presssure. **Figure 3-3** shows the AFM images of the HVB_{12}-cerasome absorbed on PDDA-PVS precursor film modified mica substrate. The HVB_{12}-cerasome nanoparticles closely packed like a stone pavement in the layer can be clearly observed in the whole area of the mica substrate in coincident with report [29-30]. It is proved that HVB_{12} functionalized cerasomes are assembled on the solid substrate without collapse due to the siloxane network on the surface. The observation also reveals that incorporated HVB_{12} does not have obviously effect on the morphorlogical stability of

cerasome.

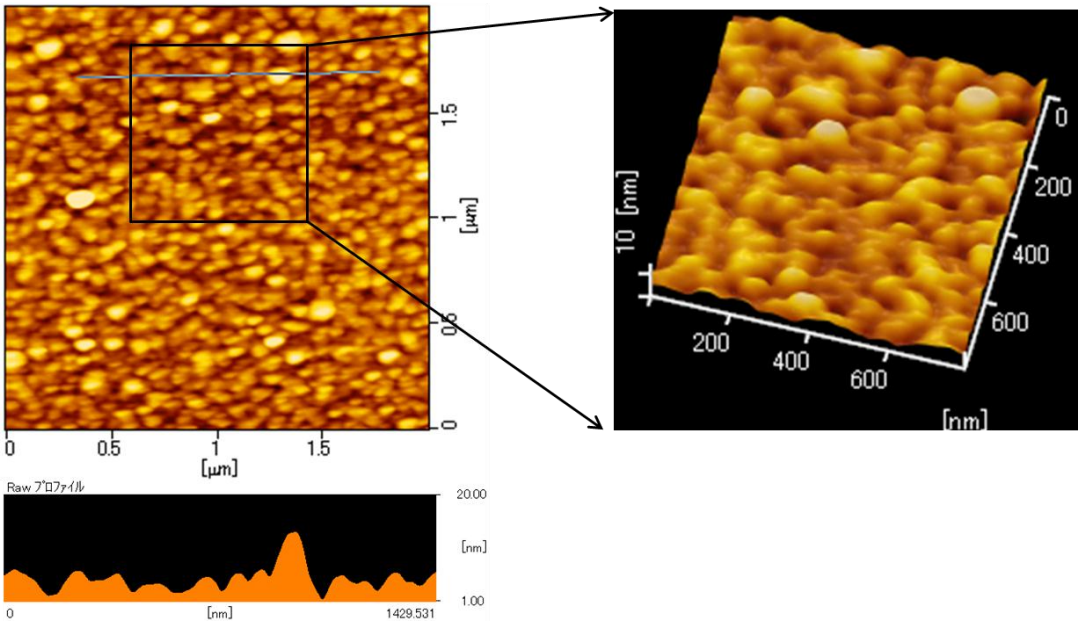

Figure 3-3. Tapping mode AFM topography for HVB_{12}-cerasome (left) and 3D topography (right) samples on fresh mica. The sample was prepared by layer-by-layer method. [cerasome forming lipids] = 1mM

3. 3. 3 Phase transition behaviors of cerasome-artificial coenzyme nanohybrid

Differential scanning calorimetry (DSC) is one of the most useful thermal analytical techniques for monitoring the phase behavior of lipid bilayer. The informations from DSC thermorgram on lipid conformation, bilayer fluidity, and the bilayer-foreign molecule interaction are obtained [31]. Therefore, the DSC response of HVB_{12} to the membrane of cerasome was evaluated. DSC thermograms of cerasome (solid line) and HVB_{12}-cerasome (dash line) are shown in **Figure 3-4**. The transition temperature (T_m) is observed at 25.5 °C for cerasome. Phase transition behavior can be described the transition of lipid bilayers from an ordered gel state at lower temperature to a more disordered liquid crystalline state at higher temperature. The enthalpy of the transition is 26.3 kJ mol^{-1}. In the cerasome which contains HVB_{12} of 0.015 mM, the transition

parameters are lightly changed. Upon addition of HVB_{12} into cerasome, the main transition endotherm is broadened and shifted to 25.6 °C associated with an increase of half-height width. The enthalpy change for the transition HVB_{12}-cerasome calculated is 25.9 kJ mol^{-1}, which is similar with that of cerasome. The phase transition from gel to liquid crystalline phase in lipid bilayer can be described as a transition from order to disorder. The slight changes of the parameters presented here predict the addition of HVB_{12} probably almost does not effect on the fluidity, disorder and mobility of the lipid bilayer [32]. It demonstrates that the lipid bilayer membrane structure of cerasome is not disturbed by HVB_{12} under this concentration.

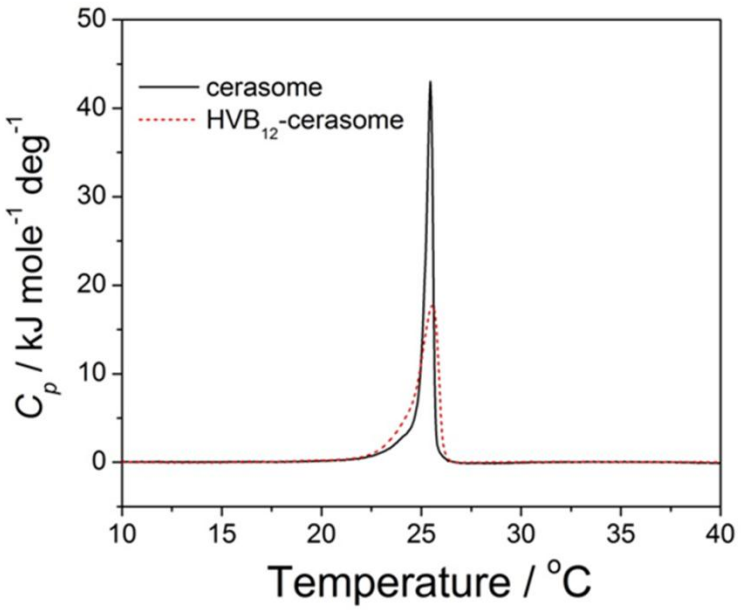

Figure 3-4. DSC thermographs of cerasome (solid line) and cerasome containing 1.5% of vitamin B_{12} in mole (dash line). [cerasome forming lipid] = 1mM.

3. 3. 4 Electrochemical properties of electrode modified with cerasome and artificial coenzyme.

The investigations on electrochemical behaviors of hydrophobic vitamin B_{12}

immobilized onto ITO, platinum electrode in aqueous solution have been carried out in non-aqueous and aqueous solution [28, 33, 34]. These studies demonstrated that HVB_{12} was electrochemically active. Here I evaluated the electrochemical properties of HVB_{12} incorporated into cerasome on glassy carbon electrode by means of cyclic voltammetry. All of the electrochemical measurements were carried out at room temperature (ca. 25 °C) close to the T_m of HVB_{12}-cerasome, 25.5 °C (**Figure 3-4**). Hisaeda et al, have clarified that HVB_{12} molecules incorporated in vesicles formed by peptide lipids were not situated in the nonpolar domain composed of the aliphatic double-chains but in the polar domain composed close to the amino acid residues [8]. Additionally, the phase transition temperature of vesicles formed by peptide lipids is primarily dependent on the packing mode of lipid molecules in their double hydrocarbon-chain domains [12]. So the electrochemical behavior of incorporated HVB_{12} is probably not influenced by the phase of lipid bilayer.

Figure 3-5 shows cyclic voltammograms recorded on HVB_{12}-cerasome/GCE (a) and cerasome/GCE (b) modified electrode in oxygen-free PBS solution (0.1 M, pH = 7). From the voltammograms on black curve it can be seen that a reversible couple of reduction-oxidation peaks at ca. -0.353 V, which are ascribed to the redox pair of Co(II)/Co(I). However, the corresponding redox potential of [Cob(II)7C_3ester]ClO_4 trapped in sol-gel modified electrode in aqueous solution is -0.42 V vs. Ag/AgCl [28]. The possible reason is that electronic state of the nuclear cobalt atom in different medium is different. Nearly no signals can be observed on CV of cerasome/GCE electrode (b) at the corresponding range of potential, declaring that cerasome is not electroactive. A single wave at 0.36 V can be seen, which is attributed to oxidation of Co(II). Whereas, the reduction peak of Co(III) cannot be observed which agrees with

the phenomenon reported by Shimakoshi et al [28]. The Co(III) atom easily forms two coordination bonds with axial ligands, which is probably hydroxyl ion (OH^-) or water (H_2O). After the axial coordination, the reduction peak of Co(III) would be broadened or shifted. Additionally, the rate of electron transfer may be too slow. As a result, the reduction peak of Co(III) is not observed in the cyclic voltammetry.

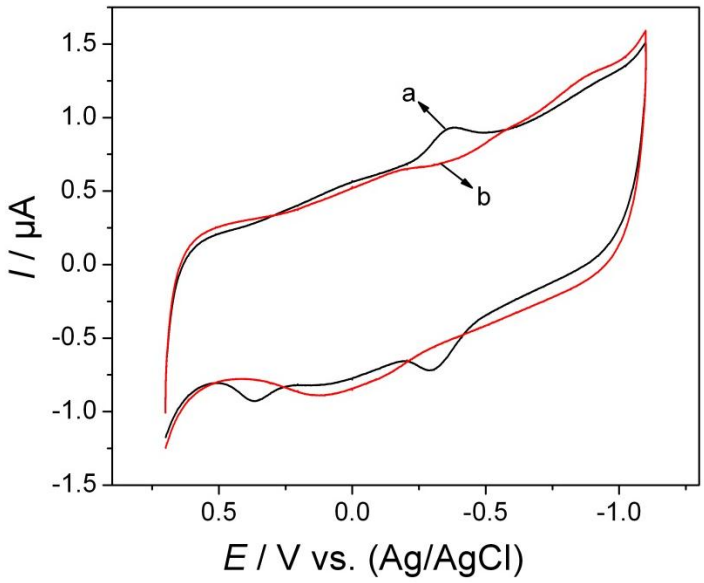

Figure 3-5. The CVs of HVB_{12}-cerasome (a) and cerasome (b) modified electrode in oxygen-free PBS buffer solution (0.1M, pH =7) containing 0.1M KCl. Scan rate: 200 mV s^{-1}.

Cyclic voltammograms of the HVB_{12}-cerasome modified GCE at various sweep rates between 0.1 and 0.6 V versus Ag/AgCl are shown in **Figure 3-6 (A)**. It is clearly observed that both cathodic and anodic peak currents intensity increase linearly proportional to scan rate shown in **Figure 3-6 (B)**. It is expected for a typical surface-controlled electrode process in the range of potential range from 0.1 to 0.6 V. According to Faraday's law, $Q = nFA\Gamma^*$ (In this equation, F, Faraday's constant; *n*, number of transferred electrons per molecule; A, the electrode area, 0.07 cm^2; Γ^*, surface coverage of eletroactive HVB_{12}; *Q*, evaluated from the integration of cathodic

peak of Co(II) in the cyclic voltammograms), the surface concentration of HVB_{12} on the HVB_{12}-cerasome modified electrode, Γ^*, could be evaluated at the scan rate of 100 mV s^{-1} was 6.72×10^{-12} mol cm^{-2}.

In this experiment, 7 μL of HVB_{12}-cerasome dispersions (0.015mM) were cast on the electrode surface. So the amount of deposited HVB_{12} on electrode was 1.1×10^{-10}mol. Thus the percentage of electroactive HVB_{12} molecules among total deposited HVB_{12} on the glassy carbon electrode was calculated to be 0.43 %, suggesting a very small part of HVB_{12} had electron exchange with electrode surface. One probable reason is some HVB_{12}-cerasomes were lost during preparation. The other reason may be the HVB_{12} molecules are sparsely distributed in cerasome according to the area percentage, 2.4%. So the electron transfer is hard to achieve through electron hopping. As the result, the HVB_{12} situated a position far away from the electrode surface cannot exchange electron with electrode surface.

The area percentage of HVB_{12} in one cerasome is calculated as follows:

The orientation of HVB_{12} situated in the lipid bilayer is not clear. The cation of HVB_{12} molecule is supposed to a cuboid with length a, width b, and height, c based on the 3D chemical structure (**Scheme 3-3**). The head area of lipid is assumed to 0.7nm^2. And the molar ratio of lipid to HVB_{12} is 100:1.5. Assuming HVB_{12} molecule with the long axis vertical to the surface of cerasome, the area (a × b) of HVB_{12} is 1.15 nm^2. If the HVB_{12} molecules are distributed evenly around cerasome, the area ratio of total lipid to total HVB_{12} in one cerasome is 100×0.7 nm^2: 1.5×1.15 nm^2 = 70:1.73. As a result, the area percentage of HVB_{12} in one cerasome is 1.73/(70+1.73) × 100% = 2.4%.

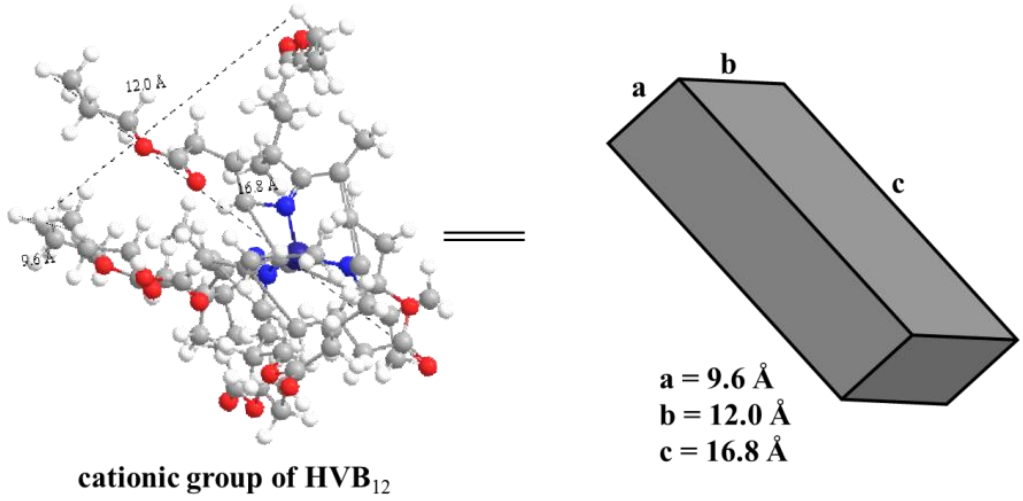

Scheme 3-3. Three dimensional structure of cationic group of hydrophobic vitamin B_{12}.

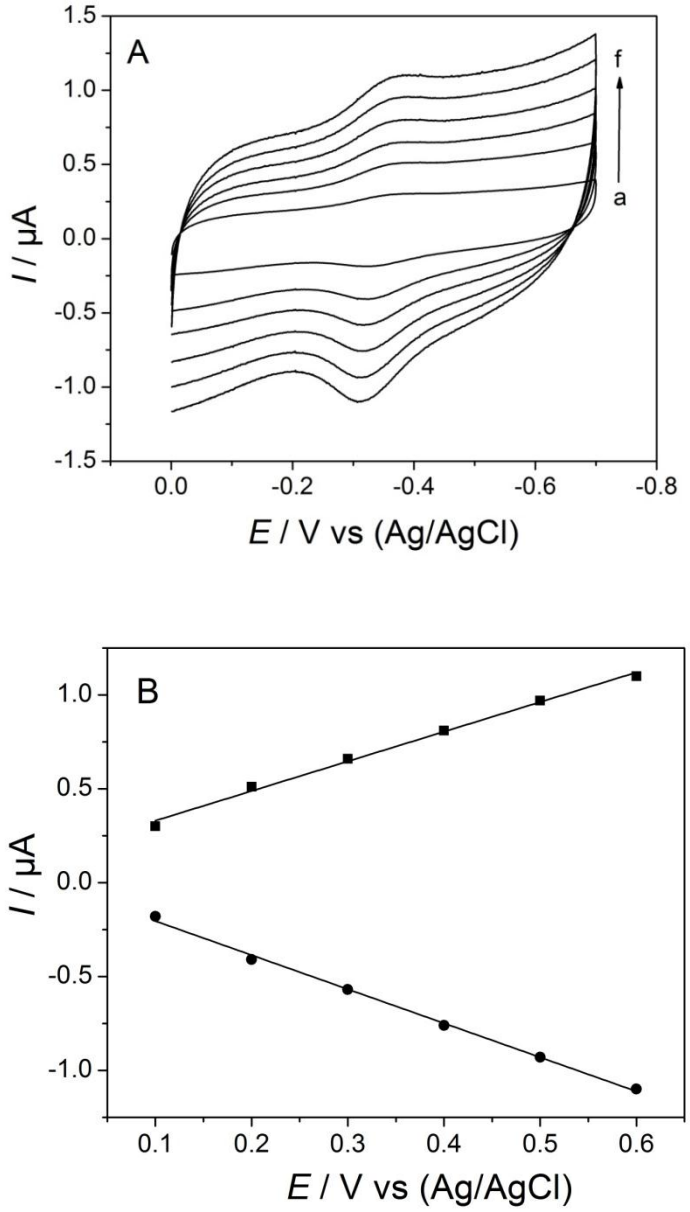

Figure 3-6. (**A**) CVs of HVB_{12}-cerasome modified electrode in PBS solution at different scan rates of 0.1 (a), 0.2 (b), 0.3 (c), 0.4 (d), 0.5 (e) 0.6 (f) V s^{-1} and (**B**) peak currents versus scan rates.

3. 3. 5 Electroanalytical behaviors of electrode modified with cerasome and artificial coenzyme.

Hydrophobic vitamin B_{12} has been found to exhibit various interesting catalytic activities because of its rich redox chemistry. I studied electrocatalytical function of

HVB_{12} trapped in cerasome toward oxygen, hydrazine and iodomethane, respectively.

3. 3. 5. 1 Electrocatalysis of HVB_{12}-cerasome/GCE modified electrode toward oxygen

Determination of dissolved oxygen has the potential interest in the fields, such as environment, industry, food, biochemistry, and clinic. There are several useful techniques, one of which is electrochemical method [35]. In this research I employed the resulting HVB_{12}-cerasome/GCE to detect the dissolved O_2 in aqueous solution. The air was used instead of pure oxygen in this experiment. As required, the PBS solution was bubbled with various volume of air with 25 ml syringe. **Figure 3-7** shows the cyclic voltammograms for reduction of O_2 at cerasome modified GCE in oxygen-free neutral electrolyte with (a) and without (b) HVB_{12}. A broad peak appears at -0.72 V on cerasome/GCE modified electrode attributable to the O_2 reduction. However, when the O_2 is in presence on HVB_{12}-cerasome/GCE modified electrode, a sharp irreversible wave at -0.48 V can be observed, which 0.24 V positively shifts. This indicates a typically electrocatalytic process of O_2 by of HVB_{12} embedded in cerasome. Moreover, the intensity of cathodic currents of HVB_{12}-cerasome modified electrode are gradually increased with the increasing of oxygen concentration, while anodic currents proceed gradual decrease during this progress (**Figure 3-8**). These results illustrates that the cobalt center of HVB_{12} in cerasome is kept well electrocatalytic activity.

As described in reports, the mechanism of O_2 reduction relied mainly upon the pH value of the medium as well as the electrode material [36, 37]. The process of O_2 reduction in aqueous solution contains two main pathways: peroxide pathway followed by either the further reduction reaction or the decomposition reaction and direct 4-electrode pathway. From the catalytic curve of a, two reduction peaks at -0.48 V and

-0.83 V, respectively are observed. This result is similar with that of electroreduction of O_2 catalyzed by natural vitamin B_{12} on an ordinary pyrolytic graphite electrode [38]. Therefore I speculated that the two reduction peaks could be related to two redox steps each involving two electrons to generate peroxide and water or OH^-, respectively.

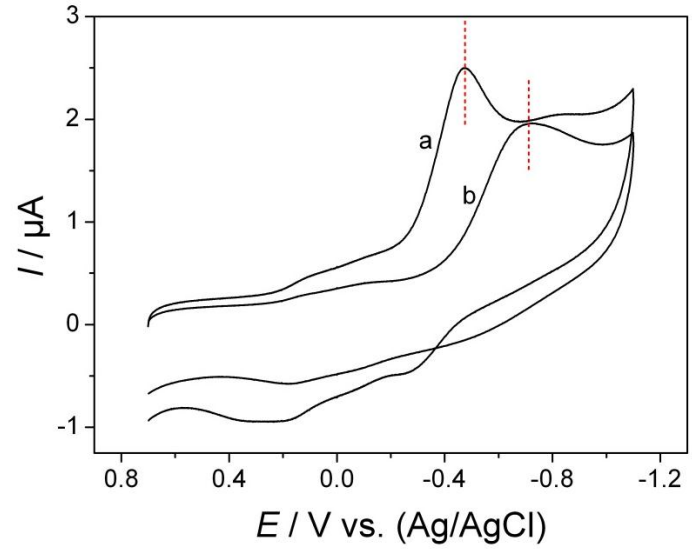

Figure 3-7. CVs of the HVB_{12}-cerasome/GCE (a) and cerasome/GCE (b) in presence of 5 ml of air in PBS buffer solution (pH = 7, 0.1 M). Scan rate: 200 mV s^{-1}.

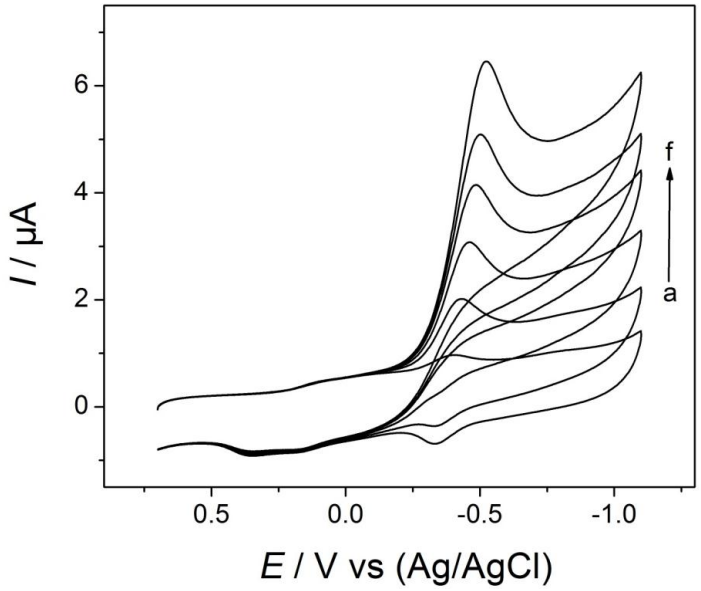

Figure 3-8. CVs of HVB_{12}-cerasome modified electrode in PBS solution (pH = 7, 0.1 M) containing various volumes of air: 0, 2, 5, 8, 12, 16 ml from a to f. Scan rate: 200 mV s^{-1}.

3. 3. 5. 2 Electrocatalytic oxidation of HVB_{12}-cerasome/GCE towards hydrazine

Hydrazine, a colorless liquid, is an important compound in chemical and pharmaceutical industries commonly used as a reducing regent and catalyst [39, 40]. Hydrazine is also applied in insecticides. Since it is widely used in environment, the detection of hydrazine becomes necessary. To evaluate electrocatalytic function and develop potent application of HVB_{12}-cerasome nanohybrid, the electrocatalytic oxidation of hydrazine at the HVB_{12}-cerasome/GCE was therefore studied by CV. **Figure 3-9 (A)** shows the electrocatalytic oxidation of hydrazine at HVB_{12}-cerasome/GCE modified electrode. The oxidation peak of hydrazine appeares at E_{pa} = 0.34 mV and an increase is observed with increasing concentration of hydrazine [41]. The calibration curve gives a linear range from 1.03 to 212.2 mM with a correlation coefficient of 0.9860 (**Figure 3-9 B**). The experimental results indicate HVB_{12}-cerasome exhibits well electrocatalytic response to hydrazine, suggesting a new method for the determination of hydrazine.

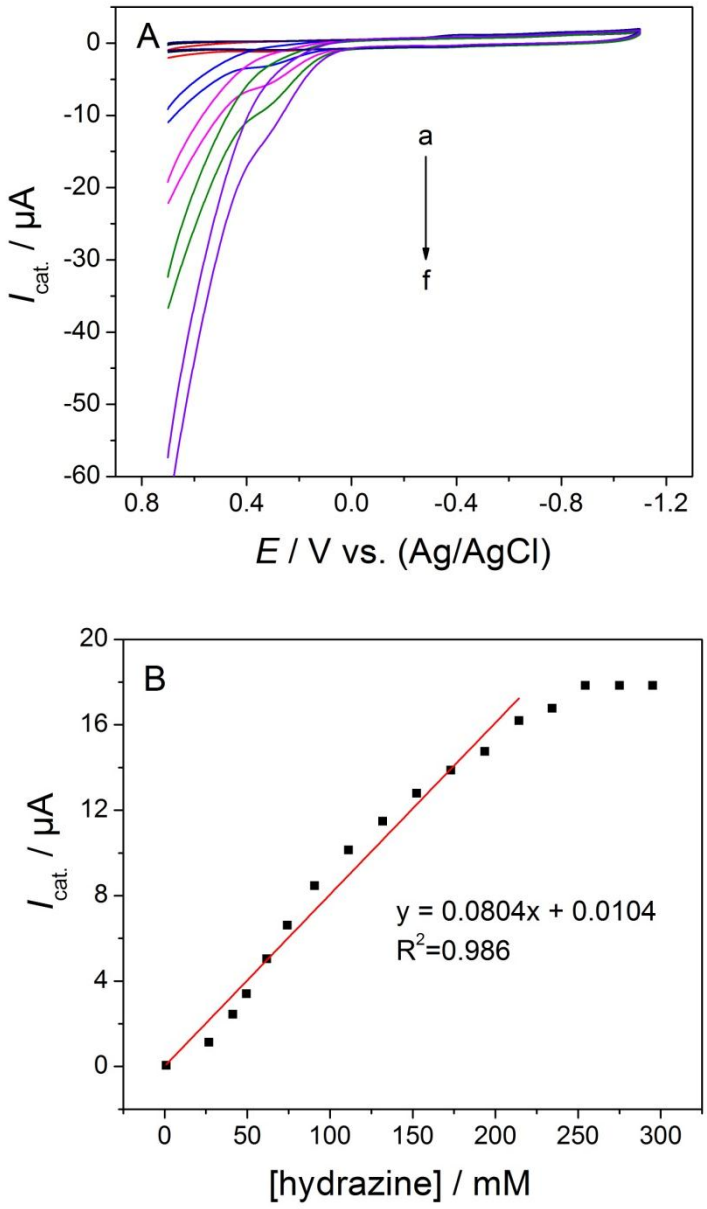

Figure 3-9. (A) The CVs of hydrazine with various concentrations on the HVB_{12}-cerasome modified electrode in PBS at 200 mV s^{-1} and **(B)** the plot of peak current versus hydrazine concentration.

3. 3. 5. 3 Electrolysis of iodomethane mediated by immobilized HVB_{12}-cerasome

Vitamin B_{12} derivatives are considered as some of the most effective catalysts for the dehalogenation of halogenated compound [42, 43]. The cobalt atom in HVB_{12} consists

three main formal oxidation states, Co(III), Co(II) and Co(I). The Co(I) in reduced HVB_{12} is a powerful nucleophile. It reacts with various organic halides to form Co(III)-alkyl intermediates through dehalogenation following homolytically cleave by electrolysis, photolysis or thermolysis to form the corresponding radical species (**Scheme 3-3**) [44, 45].

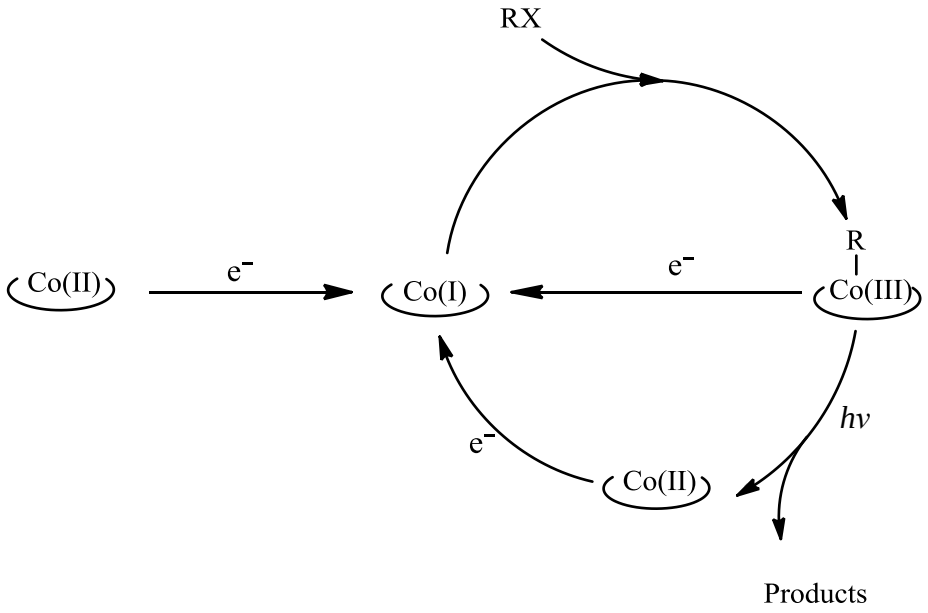

Scheme 3-3. Reaction cycles.

The electrocatalytic behaviors of HVB_{12}-cerasome/GCE toward iodomethane (CH_3I) were evaluated by cyclic voltammetry. **Figure 3-10** shows the cyclic voltammogram of electrolysis of CH_3I (32 μM) on HVB_{12}-cerasome/GCE (a) and cerasome/GCE (b). A broad reduction peak with strong current is located at ca. -1.35 V vs. Ag/AgCl, while there is no clear peak on the cerasome/GCE modified electrode at the same potential. This peak is assigned to the formation of the one-electron reduction intermediate of the Co(III)-CH_3, which is generated by the reaction between Co(I) species and CH_3I. The catalytic mechanism proposed on the electrode surface is described in following equations:

$$Co(II) + e^- \rightleftharpoons Co(I) \quad (1)$$

$$Co(I) + CH_3I \longrightarrow CH_3\text{-}Co(III) + I^- \quad (2)$$

$$CH_3\text{-}Co(III) + e^- \longrightarrow CH_3\cdot + Co(I) \quad (3)$$

First, one electron reduction for Co(II) species of HVB_{12} generates the corresponding Co(I) complex at -0.35 V, as mentioned above (equation 1). The Co(I) species acts as a potent nucleophile for methyl iodide to form an intermediate having a Co-C bond (Co(III)-CH_3) and iodide ion (equation 2). This intermediate is reduced at -1.35 V to produce methyl radical and Co(I) species through homolytic cleavage of cobalt-carbon bond (equation 3). The resulting Co(I) species further reacts with methyl iodide and the catalytic cycle in equations 2 and 3 rotates effectively. This result demonstrates the cobalt center of HVB_{12} is available to catalyze alkyl halide and the HVB_{12} incorporated in cerasome maintains the excellent catalyticactivity.

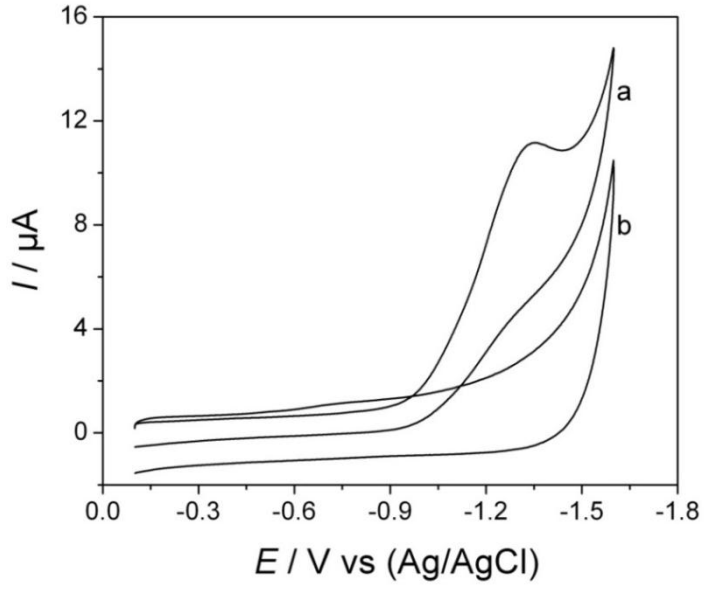

Figure 3-10. The CVs of CH_3I on HVB_{12}-cerasome (a) and cerasome (b) modified electrode in oxygen-free PBS buffer solution (0.1 M, pH =7). Scan rate: 200 mV s^{-1}.

3. 4 Conclusions

The encapsulation of artificially hydrophobic HVB_{12} into cerasome was successfully achieved according to the result of UV-vis spectra. AFM microphotograph indicates that functionalized cerasomes by HVB_{12} keep well vesicular structure even on the solid substrate. Besides, the phase transition behaviors of cerasome embedded with HVB_{12} can maintain according to the DSC thermorgram. Furthermore, this immobilized cerasome by HVB_{12} exhibits excellent electroactive property, which has sensitive response to substrates, such as iodomethane and hydrazine. As a result, the development of unique electroactive cerasome could provide a good candidate for developing enzyme-free biosensing device, and find wide potential applications in direct electrochemistry, biosensors, biocatalysis and biomedical devices.

3. 5 References

[1] Golding B T, Rao D N, in Enzyme Mechanisms, ed, by Page M I and Williams A, The Royal Society of Chemistry, London, 1987, pp 404-428.

[2] Pratt J M, in: B_{12}, ed, by Dolphin D, Wiley, New York, 1982, 1, pp 325-392.

[3] Hisaeda Y, Nishioka T, Inoue Y, Asada K, Hayashi T. Electrochemical reactions mediated by vitamin B_{12} derivatives in organic solvents. Coord. Chem. Rev. 2000; 198: 21-37.

[4] Murakami Y, Hisaeda Y, Kajihara A. Hydrophobic vitamin B_{12}. I. Preparation and axial ligation behavior of hydrophobic vitamin B12r. Bull. Chem. Soc. JPN. 1983; 56: 3642-3646.

[5] Murakami Y, Hisaeda Y, Kajihara A, Ohno T. Hydrophobic vitamin B_{12}. II. Coordination geometry and redox behavior of heptamethyl cobyrynate in nonaquaous media. Bull. Chem. Soc. JPN 1984; 57: 405-411.

[6] Murakami Y, Hisaeda Y, Kajihara A, Ohno T. Hydrophobic vitamin B_{12}. III. Incorporation of hydrophobic vitamin B_{12} derivatives into single-compartment vesicles and their alkylation in various molecular aggregates. Bull. Chem. Soc. JPN. 1984; 57: 2091-2097.

[7] Murakami Y, Hisaeda Y, Kikuchi J, Ohno T, Suzuki M, Matsuda Y, Matsuura T. Hydrophobic vitamin B_{12}. Part 6. Carbon-skeleton rearrangement via formation of host-guest complexes derived from an ‘octopus’ azaparacyclophane and hydrophobic vitamin B_{12} derivatives: a novel holoenzyme model system. J. Chem. Soc. Perkin Trans. 1988; 2: 1237-1246.

[8] Murakami Y, Hisaeda Y, Ohno T. Hydrophobic vitamin B_{12}. Part 9. An artificial holoenzyme composed of hydrophobic vitamin B_{12} and synthetic bilayer membrane

for carbon-skeleton rearrangements. J. Chem. Soc. Perkin Trans. 1991; 2: 405-416.

[9] Murakami Y, Kikuchi J, Hisaeda Y, Hayashida O. Artificial enzymes. Chem. Rev. 1996; 96: 721-758.

[10] Hisaeda Y, Masuko T, Hanashima E, Hayashi T. Organic/inorganic hybrid nanomaterials with vitamin B_{12} functions. Sci. Tech. Adv. Mater. 2006; 7: 655-661.

[11] Murakami Y, Nakano A, Fukuya K. Stable single-compartment vesicles with zwitterionic amphiphile involving amino acid residue. J. Am. Chem. Soc. 1980; 102: 4253-4254.

[12] Murakami Y, Nakano A, Yoshimatsu A, Uchitomi K, Matsuda Y. Characterization of molecular aggregates of peptide amphiphiles and kinetics of dynamic Processes performed by single-walled vesicles. J. Am. Chem. Soc. 1984; 106: 3613.

[13] Murakami Y, Kikuchi J, in Bioorganic Chemistry Frontiers, ed, by Dugas H, Springer-Verlag, Berlin, 1991; 2: 73.

[14] Bard A J. Integrated chemical system, Wiely Interscience, New York, 1994.

[15] Bedioui F, Devynck J, Charreton C D. Immobilization of metalloporphyrins in electropolymerized films: design and applications. Acc. Chem. Res. 1995; 28: 30-35.

[16] Campbell C J, Njue C K, Nuthakki B, Rusling J F. Influence of thickness on catalytic efficiency of cobalt corrin-polyion scaffolds on electrodes in microemulsions. Langmuir 2001; 17: 3447-3453.

[17] Katagiri K, Ariga K, Kikuchi J. Preparation of organic-inorganic hybrid vesicle “cerasome” derived from artificial lipid with alkoxysilyl head. Chem. Lett. 1999; 28: 661-662.

[18] Hashizume M, Kawanami S, Iwamoto S, Isomoto I, Kikuchi J. Stable vesicular nanoparticle 'Cerasome' as an organic-inorganic hybrid formed with organoalkoxysilane lipids having a hydrogen-bonding unit. Thin Solid Film 2003; 438-439: 20-26.

[19] Matsui K, Sando S, Sera T, Aoyama Y, Sasaki Y, Komatsu T, Terashima T, Kikuchi J. Cerasome as an infusible cell-friendly and serum-compatible transfection agent in a viral size. J. Am. Chem. Soc. 2006; 128: 3114-3115.

[20] Sasaki Y, Matsui K, Aoyama Y, Kikuchi J. Cerasome as an infusible and cell-friendly gene carrier: synthesis of cerasome-forming lipids and transfection using cerasome. Nat. Protocols 2006; 1: 1227-1234.

[21] Minamida D, Okada S, Hashizume M, Sasaki Y, Kikuchi J, Hosoito N, Imori T. Cerastion of magnetic cerasome through electroless plating and their manipulation using external magnetic fields. J. Sol-Gel Sci. Technol. 2008; 48: 95-101.

[22] Gu F, Hashizume M, Okada S, Sasaki Y, Kikuchi J, Imori T. Metallosomes: artificial cell membranes with ultrathin metallic surface derived from cationic cerasome through electroless plating. J. Ceram. Soc. JPN. 2008; 116: 400-405.

[23] Dai Z H, Tian W J, Yue X L, Zheng Z Z, Qi J J, Tamai N, Kikuchi J. Efficient fluorescence resonance energy transfer in highly stable liposomal nanohybrid cerasome. Chem. Commun. 2009; 2032–2034.

[24] Ikeda A, Nagano M, Akiyama M, Matsumoto M, Ito S, Mukai M, Hashizume M, Kikuchi J, Katagiri K, Ogawa T, Takeya T. Photodynamic activity of C_{70} caged within surface-cross-linked liposomes. Chem. Asian J. 2009; 4: 199-205.

[25] Liang X L, Yue H L, Dai Z F, Kikuchi J. Photoresponsive liposomal nanohybrid cerasomes. Chem. Commun. 2011; 47: 4751-4753.

[26] Katagiri K, Hamasaki R, Hashizume M, Ariga K, Kikuchi J. Size-selective organization of silica and silica-like particles on solid interfaces through layer-by-layer assembly. J. of Sol-Gel Sci. and Techno. 2004; 31: 59-62.

[27] Bangham A D, Horne R W. Negative staining of phospholipids and their structural modification by surface-active agents as observed in the electron microscope, J. Mol. Biol. 1964; 6: 660-668.

[28] Shimakoshi H, Nakazato A, Tokunaga M, Katagiri K, Ariga K, Kikuchi J, Hisaeda Y. Hydrophobic vitamin B_{12}. part 18. Preparation of a sol-gel modified electrode trapped with a vitamin B_{12} derivative and its photoelectrochemical reactivity. Dalton Trans. 2003; 11: 2308-2312.

[29] Katagiri K, Hamasaki R, Ariga K, Kikuchi J. Layered paving of vesicular nanoparticles formed with cerasome as a bioinspired organic-inorganic hybrid. J. Am. Chen. Sci. 2002; 124: 7892-7893.

[30] Katagiri K, Hamasaki R, Ariga K, Kikuchi J. Layer-by-layer self-assembling of liposomal nanohybrid “cerasome” on substrates. Langmuir 2002; 18: 6709-6711.

[31] Taylor K M G, Craig D Q M, in Liposome, 2ed, Oxford University Press, 2002, pp 79-101.

[32] Jain M K, Wu N Y, Wray L V. Drug-induced phase change in bilayer as possible mode of action of membrane expanding drugs. Nature 1975; 255: 494-495.

[33] Shimakoshi H, Tokunaga M, Kuroiwa K, Kimizuka N, Hisaeda Y. Preparation and electrochemical behaviour of hydrophobic vitamin B_{12} covalently immobilized onto platinum electrode. Chem. Commun. 2004; 50-51: 1805-1807.

[34] Ariga K, Tanaka K, Katagiri K, Kikuchi J, Shimakoshi H, Ohshimab E, Hisaeda Y. Langmuir monolayer of organoalkoxysilane for vitamin B_{12}-modified electrode. Phys. Chem. Chem. Phys. 2001; 3: 3442-3446.

[35] Lin M S, Leu H J, Lai C H. Development of vitamin B_{12} based disposable sensor for dissolved oxygen. Analytica. Chimica. Acta. 2006: 561; 164-170.

[36] Sawyer D T. Oxygen Chemistry, Oxford University Press, London, 1991.

[37] Yeager E. Dioxygen electrocatalysis: mechanisms in relation to catalyst structure. J. Mol. Catal. 1986; 38: 5-25.

[38] Zagal J H, Paez M, Paez C. Electroreduction of O_2 catalyzed by vitamin B_{12} adsorbed on a graphite electrode. J. Electroanal. Chem. 1987; 237: 145-148.

[39] Leakakos T, Shank R C. Hydrazine genotoxicity in theneonatal rat. Toxicol. Appl. Pharmacol. 1994; 126: 295-300.

[40] Umasankar Y, Huang T Y, Chen S M. Vitamin B_{12} incorporated with multi-walled carbon nanotube composite film for the determination of hydrazine. Anal. Biochem. 2011; 408: 297-303.

[41] Shimakoshi H, Tokunaga M, Babaa T, Hisaeda Y. Photochemical dechlorination of DDT catalyzed by a hydrophobic vitamin B_{12} and a photosensitizer under irradiation with visible light. Chem. Commun. 2004; 16: 1806-1807.

[42] Jabbar M A, Shimakoshi H, Hisaeda Y. Enhanced reactivity of hydrophobic vitamin B_{12} towards the dechlorination of DDT in ionic liquid. Chem. Commun. 2007; 1653-1655.

[43] Schessl H W, in Encyclopedia of Chemical Technology, ed. by Othmer K, 13, fourth ed., New York, 1995, p. 560.

[44] Schrauzer G N, Deutschz E. Reactions of cobalt (I) supernucleophiles. The alkylation of vitamin B_{12s}, cobaloximes (I), and related compounds. J. Am. Chem. Soc. 1969; 91: 3341-3350.

[45] Toscano P J, Marzilli L G. B_{12} and related organocobalt chemistry: formation and cleavage of cobalt carbon bonds. Prog. Inorg. Chem. 1984; 31: 105-204.

Chapter 4. General conclusions and future perspectives

In this thesis, I described the development of electroactive cerasome using naturally occurring enzyme and artificial coenzyme as redox molecules, and fabrication of electrochemical hybrid interfaces using these cerasomes as a platform based on glassy carbon electrode. Electrochemical functions of the resulting electrochemical interface were systematically analyzed using electrochemical techniques.

In first part, I utilized cerasome for construction of integrated modified electrode with the natural enzyme, HRP, as redox molecule. The direct electron transfer between HRPs and electrode surface were achieved. Since the cerasome was derived from traditional liposome and had a ceramic framework on the surface, it had enhanced physiochemical functions prior to the analogues, such as silica NP and common liposome. Herein, the systematical analysis of structure on cerasome, liposome and silica NP were performed by microscopies (SEM, AMF and cryo-TEM) and DSC. It turned out that cerasome coupled the structural merits of both liposome and silica NP. So cerasome exhibited well cell-friendly property induced by lipid bilayer and highly structural stability allowing for silicate framework on its surface. In addition, the electrochemical results showed that HRP/cerasome/GCE electrochemical interface exhibited well response on electrochemical signal transduction. However, electron transfer of immobilized HRP on the reference modified electrodes, silica NPs/GCE and liposome/GCE, were hardly realized resulting from the intrinsic structure defect of silica NP and liposome. In addition, the results of electrocatalytical experiments exhibited that the immobilized HRPs on cerasomes had excellent catalytic response toward H_2O_2 and $NaNO_2$.

In second part the artificial coenzyme, HVB_{12}, was used as redox molecule in place of HRP. I firstly incorporated HVB_{12} into cerasome to obtain the electroactive cerasome. The results of DSC and UV-vis spectra indicated the HVB_{12} was embedded into the lipid bilayer membrane of cerasome, and the lipid bilayer membrane structure of cerasome was still maintained. The AFM microphotograph proved that the morphological structure of cerasome was not destroyed. Cerasome kept original morphology even on solid surface after incorporation of HVB_{12}. In addition, HVB_{12}-cerasome nanohybrids modified glassy carbon electrode had excellent electrocatalytical property, which efficiently detected the various substrates, such as, hydrazine, iodomethane in aqueous solution.

Summarily, I successfully developed a novel cerasome with well electroactivity, and clarified its potential application as the platform for fabrication of electrochemical interface. Electrochemical experiments indicated that the electron exchange was realized between the immobilized redox molecules on cerasome and electrode surface, exhibiting excellent electrocatalytic properties. The present work would serve as a useful guidepost for creating highly sensitive and innovative biosensing devices, molecular communication device, etc.

Based on the findings of this research, it is suggested to extend to the following studies:

(1) Construction of electrochemical interface using membrane protein.

As we know, the functions of the larger portion of membrane proteins, such as the interaction with membrane lipids, are still not understood, because membrane proteins are pretty difficult to study due to their hydrophobic and amphiphilic nature comparing

with water-soluble proteins [1, 2]. Thus, the characterization of membrane proteins and the modulation of their functions are still great challenges [2]. The artificial planar lipid bilayer is a powerful tool for investigation on the function of membrane proteins. Yet, they are not widely utilization because of their low stability and reproducibility [1]. Since the cerasome has more stable morphology than the traditional liposomes because of the siloxane network on the surface, it makes this study possible. As a result, it is meaningful to associate cerasome with membrane protein.

(2) Enhancement of electric conductivity of cerasome.

From the results of electrochemistry, only a small proportion of immobilized redox molecules (HRP or HVB_{12}) are electroactive. It is probably due to the poor conductivity of cerasome. Therefore, improvement of electric conductivity of cerasome is expected to increase the proportion of redox molecules and enhance the performance of electrochemical interface. To resolve this problem, one method is immobilization of cerasome by ionic liquids. As previous research, it was found that polymeric ionic liquids were good matrixes for enzyme immobilization, such as hemoglobin, because of its merits of biocompatibility and inherent conductivity [3]. In view of this, the function of cerasome can be greatly improved after introduction of structure of ionic liquid.

(3) Fabrication of interface between molecular information and electric information.

This work not only extended the application of cerasome in electrochemical field but also provided a potential model for fabrication of electron transfer system, whereby, molecular signal can be transferred into electric signal. Molecular communication is a new communication paradigm using molecules as information carriers, inspired by biological signal transduction system [4]. It is a challenging and interdisciplinary

research topic including information, biological, and materials science fields. The concept of molecular communication has been proposed by the information scientists and actively investigated theoretically, but its demonstration is an unsettled problem up to the present time. It is necessary to construct the interface between the molecular communication and the conventional electronic communication, which is capable of transforming molecular information signal into an electrochemical signal in real time (**Figure 4-1)** [5]. Such interface could offer a convenient way to deeply study and well understand the molecular communication.

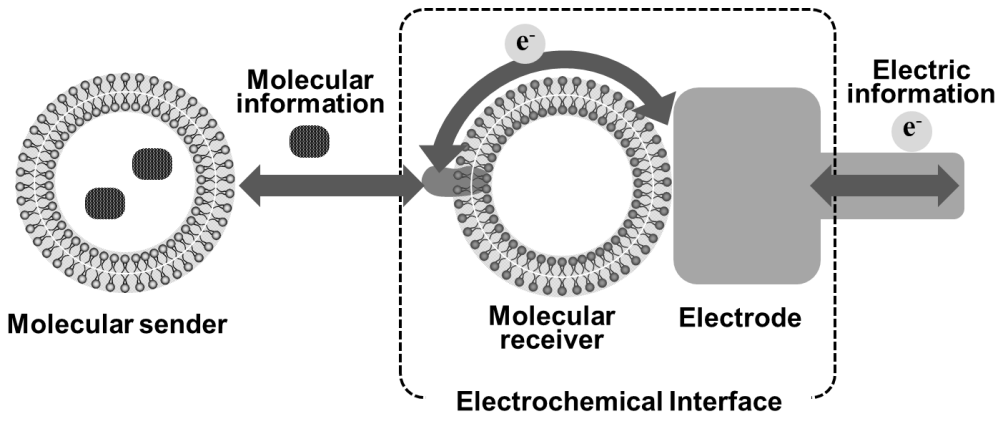

Figure 4-1. Illustration of interface between molecular information and electric information [5].

References

[1] Funakoshi K, Suzuki H, Takeuchi S. Lipid bilayer formation by contacting monolayers in a microfluidic device for membrane protein analysis. Anal. Chem. 2006; 78: 8169-8174.

[2] Melin F, Hellwig P. Recent advances in the electrochemistry and spectro-electrochemistry of membrane proteins. Bio. Chem. 2013; 394: 593-609.

[3] Zhang Q, Lv X, Qiao Y, Zhang L, Liu D L, Zhang W, Han G X, Song X M. Direct electrochemistry and electrocatalysis of hemoglobin immobilized in a polymeric ionic liquid film. Electroanalysis 2010; 22: 1000-1004.

[4] Moritani Y, Hiyama S, Suda T. Proc. Frontiers in the convergence of bioscience and information technology 2007; 839.

[5] Kikuchi J, Sugimoto M. Molecular communication-bio-inspired information and communication technology in next generation. Chemical Industry 2013; 64:649-654.

List of Abbreviation

T_m	Phase transition temperature
ΔH	Enthalpy change
I_p	Isoelectric point
E_{pa}	Anodic peak potential
E_{pc}	Cathodic peak potential
CV	Cyclic voltammetry
CD	Circular dichrosim
SEM	Scanning electron microscopy
AFM	Atomic force microscopy
DET	Direct electron transfer
DSC	Differential scanning calorimetry
GCE	Glassy carbon electrode
Cyro-TEM	Cryogenic transmission electron microscopy
LUV	Binary large unilamellar vesicles
M41S	Mesoporous sieves
HRP	Horseradish peroxidase
HVB_{12}	Hydrophobic vitamin B_{12}
Silica NP	Silica nanoparticle
TEOS	Tetraethylorthosilicate
DMPC	1, 2-dimyristoyl-sn-glycero-3-phosphocholine
DMPG	1, 2-dimyristoyl-sn- glycerol-3-phosphoglycerol
PVS	Potassium poly(vinyl sulfate)

PDDA	Poly(diallyldimethylammonium chloride)
TFA	Trifluoroacetic acid
PBS	Phosphate buffer solution

Acknowledgements

I would like to take this opportunity to thank all the persons who have contributed in the different aspects of my study. They have all made it possible for me to commence and complete this doctoral work. I would like to acknowledge and commend them for their assistance that has worked towards the success of my research work.

I am deeply grateful to my supervisor, Prof. Jun-ich Kikuchi (Department of Materials Science, Graduate School of Materials Science, Nara Institute of Science and Technology) for his enthusiastic guidance, comments, discussions and encouragement in successive throughout the three-year course of my doctoral study.

I would like to express my very great appreciation to Prof. Xi-Ming Song and Assoc. Prof. Qian Zhang (College of Chemistry, Liaoning Provincial Key Laboratory for Green Syntheses, Liaoning University, Shenyang China) for his valuable and constructive suggestions during the planning and development of this research work. Especially, Prof. Qian Zhang's willingness to give his time to revision of my article has been very much appreciated.

I am also very grateful to Prof. Yoshio Hisaeda (Department of Applied Chemistry, Graduate School of Engineering, Kyushu University) for his a lot of useful comments and suggestions about my research work.

Especially, give my appreciation to Prof. Michiya Fujiki, Prof. Shun Hirota and Assoc. Prof. Takuya Nakashima (Department of Materials Science, Graduate School of Materials Science, Nara Institute of Science and Technology) for their scientific advices and knowledge and many insightful discussions and suggestions about the research.

I would like to express my deep gratitude to Assist. Prof. Kazuma Yasuhara and

Assist. Prof. Keishiro Tahara (Department of Materials Science, Graduate School of Materials Science, Nara Institute of Science and Technology) for their patient assistance, enthusiastic encouragement and useful critiques of this research work.

I would also like to extend my thanks to the technician, Sakiko Fujita (Department of Materials Science, Graduate School of Materials Science, Nara Institute of Science and Technology) for her technical assistance in cryo-TEM observations.

I would like to acknowledge the contribution of students (Biomimetic Material Science Laboratory, Department of Materials Science, Graduate School of Materials Science, Nara Institute of Science and Technology), Drs. Ke Xu, Hao Fei, Manami Tsukamoto and all other members in our laboratory with whom I have worked during this doctoral work.

Finally, I wish to thank my parents and my sisters for their constant support, especially, my husband, Wu Sun, who always encourage and help me to over the difficulties throughout my doctoral study.

List of publications

Some publications originated from this study were listed follows:

1. **Construction of Molecular Communication Interface Formed with Cerasome and Hydrophobic Vitamin B_{12} on a Glassy Carbon Electrode.**

   Yun Qiao, Keishiro Tahara, Qian Zhang, Xi-Ming Song, Yoshio Hisaeda, Jun-ichi Kikuchi, *Chem. Lett.*, accepted.

2. **Cerasome: Biocompatible Matrix for the Electrochemical Signal Transmission of Enzyme**

   Yun Qiao, Keishiro Tahara, Qian Zhang, Xi-Ming Song, Jun-ichi Kikuchi, *Biomaterials*, to be submitted.

Related works

1. Fabrication of Biocompatible and Conductive Platform Based on Single Stranded-DNA/Graphene Nanocomposite for Direct Electrochemistry and Electrocatalysis.

Qian Zhang, Yun Qiao, Fei Hao, Ling Zhang, Shu-yao Wu, Ying Li, Jing-hong Li, Xi-ming Song, *Chem. Eur. J.*, 2010. 16(27), 8133-8139.

2. Direct Electrochemistry and Electrocatalysis of Hemoglobin Immobilized in a Polymeric Ionic Liquid Film.

Qian Zhang, Xue Lv, Yun Qiao, Ling Zhang, Da-Liang Liu, Wei Zhang, Guang-Xi Han, Xi-Ming Song. *Electroanalysis*, 2010, 22(9), 1000-1004.

3. Direct Electrochemistry and Electrocatalysis of Horseradish Peroxidase Immobilized on Water Soluble Sulfonated Graphene Film via Self-assembly.

Qian Zhang, Yun Qiao, Ling Zhang, Shu-yao Wu, Hua Zhou, Jing-wei Xu, Xi-Ming Song. *Electronanalysis*, 2010, 23(4), 900-906.